

Master's Thesis
석사 학위논문

A Non-precious Metal Oxide based Bi-functional
Catalyst for Oxygen Reduction and Evolution
Reactions in Alkaline medium

Taeun Ahn (안 태 은 安 台 恩)

Department of Energy Systems Engineering
에너지 시스템 공학 전공

DGIST

2014

Master's Thesis
석사 학위논문

A Non-precious Metal Oxide based Bi-functional
Catalyst for Oxygen Reduction and Evolution
Reactions in Alkaline medium

Taeun Ahn (안 태 은 安 台 恩)

Department of Energy Systems Engineering

에너지 시스템 공학 전공

DGIST

2014

A Non-precious Metal Oxide based Bi-functional Catalyst for Oxygen Reduction and Evolution Reactions in Alkaline medium

Advisor : Professor Sangaraju Shanmugam

Co-advisor : Doctor Soonhyun Kim

by

안태은

Department of Energy Systems Engineering
DGIST

A thesis submitted to the faculty of DGIST in partial fulfillment of the requirements for the degree of Master of Science in the Department of Energy Systems Engineering. The study was conducted in accordance with Code of Research Ethics¹

12. 10. 2013

Approved by

Professor Sangaraju Shanmugam _____ (Signature)
(Advisor)

Doctor Soonhyun Kim _____ (Signature)
(Co-Advisor)

¹ Declaration of Ethical Conduct in Research: I, as a graduate student of DGIST, hereby declare that I have not committed any acts that may damage the credibility of my research. These include, but are not limited to: falsification, thesis written by someone else, distortion of research findings or plagiarism. I affirm that my thesis contains honest conclusions based on my own careful research under the guidance of my thesis advisor.

A Non-precious Metal Oxide based Bi-functional Catalyst for Oxygen Reduction and Evolution Reactions in Alkaline medium

Taeun Ahn (안 태 은 安 台 恩)

Accepted in partial fulfillment of the requirements for the degree of
Master of Science

12. 10. 2013

Head of Committee _____(인)

Prof. Sangaraju Shanmugam

Committee Member _____(인)

Dr. Soon-Hyun Kim

Committee Member _____(인)

Prof. Seung-Tae Hong

MS/ES
201224015

안 태 은. Tae-eun Ahn. A Non-precious Metal Oxide based Bi-functional Catalyst for Oxygen Reduction and Evolution Reactions in Alkaline medium. Department of Energy Systems Engineering. 2014. 61p. Advisors Prof. Sangaraju Shanmugam, Co-Advisors Dr. Kim, Soonhyun.

ABSTRACT

Finite fossil fuels and destroyed nature make us to rely on develop renewable energy resources. One of the promising energy systems is metal-air battery which meets drawbacks of traditional metal-ion battery. The redox reaction of metal and oxygen (O_2) in air generates electrical energy. A key issue of metal-air battery is to improve the efficiency of cathode that occur redox reaction of O_2 such as oxygen reduction reaction (ORR) and oxygen evolution reaction (OER).

Platinum (Pt), Iridium (Ir) and Ruthenium (Ru) oxides are commonly used as bi-functional catalysts for ORR and OER. These materials have limitations of cost and quantity, and they have to be overcome for commercialization. To satisfy these limitations, cobalt oxide is studied with diverse approaches in this work.

Doped with manganese (Mn) and nitrogen (N) showed increasing performance for both reactions and cobalt hydroxide explains the mechanism of OER because ORR has been already reported many times. Morphology, structure, electronic property and electrochemical activities of all materials will be discussed. A final goal is to find good bi-functional catalysts with understanding of its reaction.

Keywords:

Bi-functional catalyst, Oxygen reduction reaction, Oxygen evolution reaction, Cobalt oxide

Contents

Abstract	i
List of contents	ii
List of table	iii
List of figures	iv
I . INTRODUCTION	1
1.1. Foreword	1
1.2. Characteristics of metal-air batteries	2
1.2.1. Advantages & disadvantages of metal-air batteries	2
1.2.2. Basic principles of metal-air batteries	4
1.3. Studies of bi-functional catalysts	8
1.3.1. Various types of bi-functional catalysts	8
1.3.2. ORR & OER studies	10
1.4. Theoretical background	14
1.4.1. Concept of doping	14
1.4.2. Characteristic of materials	15
1.5. Objectives of work	16
II . EXPERIMENTAL	18
2.1. Chemicals	18
2.2. Synthesis of Graphene oxide (GO)	18
2.3. Synthesis of catalysts	19
2.3.1. Preparation of cobalt oxide/GO	19
2.3.2. Preparation of manganese doped cobalt oxide/GO	19
2.3.3. Preparation of nitrogen doped cobalt oxide/GO	19
2.3.4. Preparation of cobalt hydroxide/GO	20
2.4. Characterizations	
2.4.1. Morphological analysis	20
2.4.2. Elemental characterization	21
2.4.3. Electrochemical studies	21

III. RESULTS \$ DISCUSSIONS	22
PART 1: Studies of catalysts with different doping	
3.1. Morphology studies of catalysts	22
3.2. Structural studies of catalysts	22
3.3. Chemical and electronic properties of catalysts	25
3.4. Electrochemical activities of catalysts	27
3.4.1. Oxygen reduction reaction activities	27
3.4.2. Oxygen evolution reaction activities	30
3.4.3. Evaluation for bi-functional catalyst	31
 PART 2: Studies of OER mechanism	
3.5. Comparison of catalysts morphologies	32
3.6. Comparison of catalysts structure	32
3.7. Comparison of chemical and electronic properties	36
3.8. Electrochemical studies	38
3.8.1. Oxygen reduction reaction activities	38
3.8.2. Oxygen evolution reaction activities	40
 IV. CONCLUSIONS	44
 REFERENCES	45
 국문 요약문	51

List of table

Table 1. Basic properties of cobalt oxide, manganese oxide and graphene	16
---	----

List of figures

Fig 1. The composition and reaction of metal-air battery	3
Fig 2. The various types of metal-air batteries	4
Fig 3. The mechanism of ORR on carbon surface	12
Fig 4. The mechanism of OER comes from water oxidation by solar energy	13
Fig 5. Different types of doping structure explained by energy band	15
Fig 6. TEM images of $\text{Co}_3\text{O}_4/\text{rGO}$, $\text{MnCo}_2\text{O}_4/\text{rGO}$ and $\text{Co}_3\text{O}_4/\text{NrGO}$	23
Fig 7. XRD patterns of $\text{Co}_3\text{O}_4/\text{rGO}$, $\text{MnCo}_2\text{O}_4/\text{rGO}$ and $\text{Co}_3\text{O}_4/\text{NrGO}$	24
Fig 8. XPS survey spectra of $\text{Co}_3\text{O}_4/\text{rGO}$, $\text{MnCo}_2\text{O}_4/\text{rGO}$ and $\text{Co}_3\text{O}_4/\text{NrGO}$	25
Fig 9. Co 2p spectra of $\text{Co}_3\text{O}_4/\text{rGO}$, Mn 2p spectra of $\text{MnCo}_2\text{O}_4/\text{rGO}$ and N 1s spectra of $\text{Co}_3\text{O}_4/\text{NrGO}$	26
Fig 10. RDE traces and Koutechy-Levich plot of $\text{Co}_3\text{O}_4/\text{rGO}$, $\text{MnCo}_2\text{O}_4/\text{rGO}$ and $\text{Co}_3\text{O}_4/\text{NrGO}$	28
Fig 11. ORR comparison of $\text{Co}_3\text{O}_4/\text{rGO}$, $\text{MnCo}_2\text{O}_4/\text{rGO}$ and $\text{Co}_3\text{O}_4/\text{NrGO}$	29
Fig 12. Tafel plot of the three catalysts and mass activities of that at 0.8 V vs.RHE	30
Fig 13. OER comparison of $\text{Co}_3\text{O}_4/\text{rGO}$, $\text{MnCo}_2\text{O}_4/\text{rGO}$ and $\text{Co}_3\text{O}_4/\text{NrGO}$	31
Fig 14. SEM images of $\text{Co}(\text{OH})_2/\text{rGO}$ and $\text{Co}_3\text{O}_4/\text{rGO}$	34
Fig 15. TEM images of $\text{Co}(\text{OH})_2/\text{rGO}$ and $\text{Co}_3\text{O}_4/\text{rGO}$	34
Fig 16. EDS images of $\text{Co}(\text{OH})_2/\text{rGO}$ and $\text{Co}_3\text{O}_4/\text{rGO}$	35
Fig 17. XRD patterns of $\text{Co}(\text{OH})_2/\text{rGO}$ and $\text{Co}_3\text{O}_4/\text{rGO}$ and the structure of $\text{Co}_3\text{O}_4/\text{rGO}$	36
Fig 18. XPS survey spectra of $\text{Co}(\text{OH})_2/\text{rGO}$ and $\text{Co}_3\text{O}_4/\text{rGO}$	37
Fig 19. Co 2p spectra and O 1s spectra of $\text{Co}(\text{OH})_2/\text{rGO}$ and $\text{Co}_3\text{O}_4/\text{rGO}$	38
Fig 20. RDE traces and Koutechy-Levich plot of $\text{Co}(\text{OH})_2/\text{rGO}$ and $\text{Co}_3\text{O}_4/\text{rGO}$	40
Fig 21. The mechanism of OER on the surface of cobalt particles in alkaline solution	42
Fig 22. OER activities of $\text{Co}(\text{OH})_2/\text{rGO}$ and $\text{Co}_3\text{O}_4/\text{rGO}$	43

I . INTRODUCTION

1.1. Forewords

Interest in renewable energy has been increasing because of the depletion of fossil fuels and the need to protect the environment. First, fossil fuels are finite. Second, nature has been destroyed by industry, and this makes environmental-friendliness an essential factor of new technologies. To satisfy both requirements, many kinds of alternative energy sources are promised such as metal-air batteries.

Traditional rechargeable metal-ion batteries are considered as the most promising energy technology, but they have several problems that prevent them from meeting the demands of commercialization¹. On the other hands, there is an approach to improve the development of metal-ion batteries. These batteries, called metal-air batteries, are considered oxygen reduction reaction (ORR) and oxygen evolution reaction (OER) at the cathode. It means that metal-air batteries, can also generate electrical energy; even more important. They much stronger point that it reacts in air: the redox reaction between metal and the oxygen in air. There is no need for specific fuel and continuous conversion of oxygen and water lead metal-air battery the ideal energy systems².

Oxygen reduction reaction (ORR) and oxygen evolution reaction (OER) occur at the cathode of metal-air batteries. ORR and OER are more difficult processes than reduction and oxidation reactions such as hydrogen because of lower exchange current density and higher over-potentials. And, many kinds of materials which have been used for catalysts are expensive and scarce, leading to difficulties in commercialization. Research for bi-functional catalyst that can be applied to not only ORR but also OER has been taken center stage recently. The main issue of bi-functional catalyst is suitable cost and affordable materials for commercialization with high performance.

Platinum (Pt), Iridium (Ir) and Ruthenium (Ru) oxides were used as bi-functional catalyst with the

problems of cost and acquisition^{3,4}. Cobalt oxide is one of the promising material to meet these problems. Using not only cobalt oxide but also a supporting material such as graphene can improve the efficiency of ORR and OER. Cobalt oxide and graphene hybrid was synthesized by hydrothermal process to form a spinel structure to enhance the performance⁵⁻⁸. In addition to, doping with other atoms such as manganese (Mn) in cobalt oxide and nitrogen (N) in grapheme oxide showed higher activities for ORR and OER.

Nowadays, diverse approaches to improve the performance of ORR and OER have been studied⁹. ORR and OER play an important role in renewable energy systems, but have to be improved to be commercialized. Still, it requires much effort and research on development of bi-functional catalyst. With continuous research, it can be one of the most important and precious energy resources for the future.

1.2. Characteristics of metal-air batteries

The first metal-air battery technology was introduced about 20 years ago. The first experiment of metal-air battery was made by Abraham et al. in 1996¹⁰, it was composed of Lithium (Li) metal anode, Li conductive organic polymer electrolyte membrane and a carbon composite electrode. In their research, they proved that metal-air battery has much higher energy densities than those of conventional metal-ion battery. But, it could not attract wide attention. The Bruce groups, who revisited metal-air battery again in 2006, showed interesting electrochemical performance for practical applications¹¹. Based on their research, metal-air battery was started developing actively in recent years..

1.2.1. Fundamental principles of metal-air batteries

A metal-air battery is composed of a metal anode, an air electrode and a separator soaked in metal-ion conduction electrolyte as shown in Fig. 1¹². The basic reactions are divided by processes such as discharge and charge.

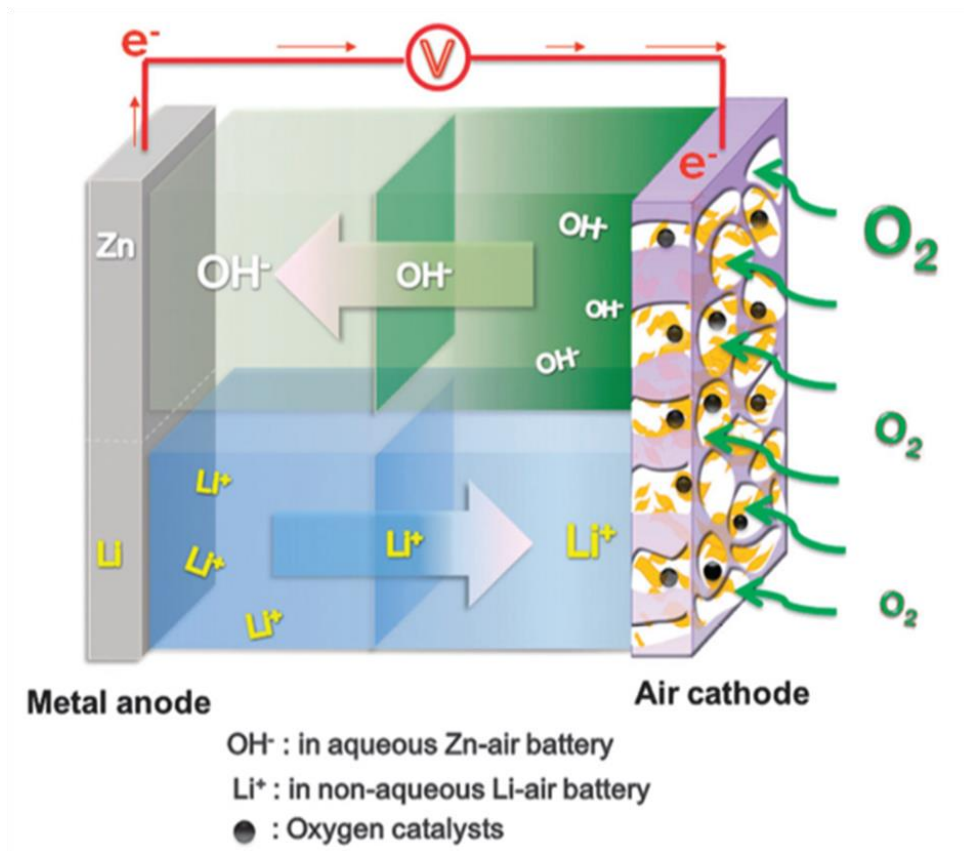


Fig. 1. The composition and reaction of metal-air battery

A. Discharge process

The anode, metal oxide electrode, is oxidized and releases electrons to external circuit and the electrons that are from the anode are accepted by the oxygen at cathode. This reaction makes an oxygen-containing species. The reduced oxygen species and dissociated metal ions migrate across the electrolyte, and it is combined to form metal oxides.

B. Charge process

It is reverse to discharge process. During charging, metal at anode is plated and oxygen is evolved at cathode.

1.2.2. Various types of metal-air batteries

Metal-air batteries are categorized by the nature of electrolytes such as aqueous or non-aqueous.

Occasionally, aqueous and non-aqueous are mixed for electrolytes and solid-state electrolyte also can be used. Various types of electrolytes of metal-air batteries are shown in Fig 2¹¹.

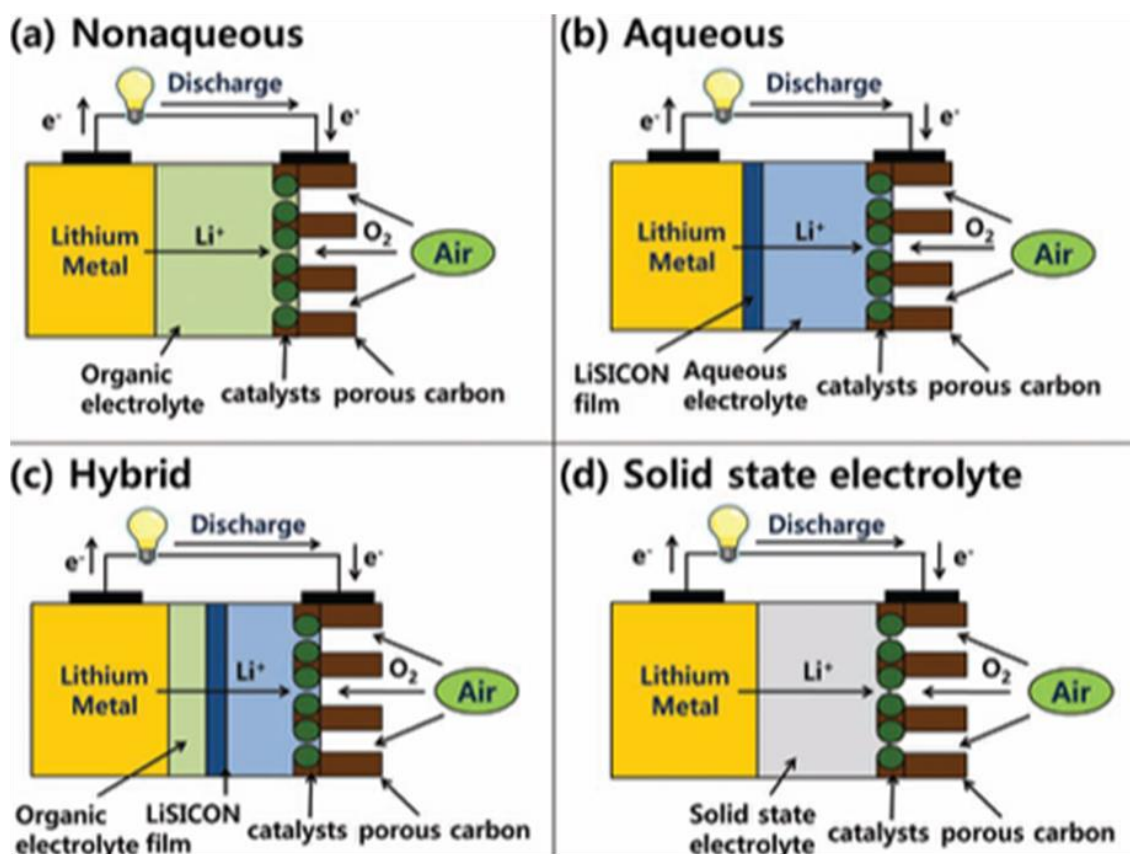
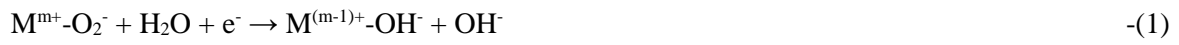


Fig. 2. The various types of metal-air batteries¹¹

A. Aqueous electrolyte

An aqueous electrolyte based system has more developed than other electrolyte because of electrochemical activities. The electrochemical reaction kinetics of oxygen is generally slow in aqueous electrolyte, when without catalysts. Alkaline solutions are commonly applied for aqueous metal-air batteries, because acid solutions make electrode to lead to severe corrosion. The ORR and OER processes in the aqueous electrolyte are divided into several steps¹³. The electrochemical approach of ORR and OER, the conversion of oxygen, is very complicated and difficult to describe because of its

strong irreversibility, and the reaction process involved multi step electron-transfer processes. Also, ORR and OER are classified with types of catalysts such as metals and metal oxides. Its surface decides a four-electron pathway or two-electron pathway of ORR. Different electron transfer pathways follow the same principle, but with a different charge distribution. In case of metal oxide has limiting steps of the ORR, which make electronic structure in metal oxide important to control the catalytic activities. The ORR pathways and mechanisms vary with the catalytic materials and electronic structure¹³⁻¹⁶. ORR of metal oxide is shown as:

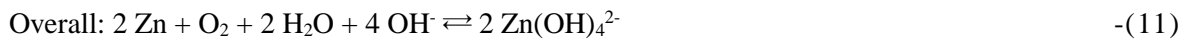


Not only mechanism of ORR but also that of OER is likely to change depending on the electrode materials. Oxygen is generally evolved from surface of metal oxide, so changeable valance state of metal ion is important for oxygen evolution reaction^{15,17,18}. One mechanism of OER in alkaline electrolyte is shown as:



The above mechanisms of ORR and OER are based on general metal oxide catalyst, and simple

mechanisms of ORR and OER of specific metal oxide such as zinc-air batteries are written as¹⁹ :



By understanding the mechanism of ORR and OER, the most important point of metal-air battery in aqueous electrolyte is the rechargeability.

B. Non-aqueous electrolyte

It is similar to conventional metal-ion batteries with same components such as metal anode that plays a role as the ion source, metal oxides cathode and ion salt dissolved in aprotic solvents as electrolytes. One difference is that metal-air battery is open system to obtain the oxygen from the air.

The reaction mechanisms in non-aqueous electrolyte have been studied for long times. The first study was introduced by Abraham et al., and Bruce group also demonstrated the similar mechanism. Recently, Laoire et al. carried out a fundamental study of the reaction mechanisms based on electrochemical analysis and XRD experiments^{20,21}. All of their study has common tendency that oxygen reduction reaction proceeds in a stepwise fashion to form O_2^- , O_2^{2-} , and O^{2-} as products by steps:

(metal= Li, is used as electrode)



Above reaction, cathode reaction, proceeds through a one electron reversible process with the O_2/O_2^- redox couple in electrolytes. Compare to ORR, in the reverse charging process, OER pathway also can be drawn that oxidation of Li_2O_2 . The OER process in non-aqueous electrolyte in other in different process was supported by Shao-Horn and McCloskey et al²²⁻².



The ORR and OER processes can be influenced by electrolytes, electrode materials, oxygen pressure, and even electrochemical stressing. The target to meet is to find out the best conditions and apply to applications.

1.2.3. Advantages & disadvantages of metal-air batteries

Metal-air batteries have more strong-points compared with conventional metal-ion batteries. For example, it has a high energy density that is the most important issue in the fields of capacitors. And, it shows the flat discharge voltage and long shelf life. From the point of view of non-performance, it has non toxic and low cost²⁵.

On the other hands, metal-air batteries have several problems to overcome to successful commercialization. It depends on environmental conditions such as electrolyte flooding which limits power output. It is limited on power density and operating temperature range. In case of metal electrode, the metal peroxide can be reacted with the electrolyte solvents and the environment, and reacted sensitively to water and CO_2 penetration²⁶.

With maintaining the advantages, metal-air batteries have to overcome the many tasks for performance. Based on advantages and disadvantages of metal-air batteries, the factors that affect performance are categorized. Above mentioned, some metals are unstable in water and react with the electrolyte to corrode the metal, resulting in self-discharge. And, metal-air batteries show sharp voltage

drop with increasing current due to oxygen diffusion limitations. Since metal-air batteries are open systems, absorption of CO₂ results in crystallization of carbonate in the air cathode electrode with clogging pores and decreasing performance. By these two factors, It is certain that air cathode that is the site for ORR and OER has to be improved. To improve the efficiency of ORR and OER at the cathode, catalysts which are composed of the most effective parts of electrode resulting in performance, and named as bi-functional catalyst has to be researched^{27,28}.

1.3. Studies of bi-functional catalysts

Bi-functional catalyst which is related to electro-catalysis of oxygen has been demonstrated to be crucial for improving the power density, cycling capability, and energy conversion efficiency of metal-air batteries^{3,4}. Because of similar principles of ORR, many catalytic materials for fuel cells could also serve in metal-air batteries, and it enhances the strategies and techniques for bi-functional catalyst more easily. Diverse bi-functional catalysts already have been used, and they can be categorized by characteristics of materials such as transition metal, carbon materials, metal-oxide hybrid, metal with doped materials, conductive polymers and noble metals. During decades, noble metal, alloys and oxides are the best materials for bi-functional catalysts^{24,29}. But, these are run into the limits such as cost and amounts. Its limitation leads active researches to find out the attractive materials for bi-functional catalysts.

1.3.1. Various types of bi-functional catalysts

Above mentioned, many materials can be categorized by its characteristics.

A. Metal, alloys, and oxides

One of the metal, Platinum (Pt), is the most effective catalyst to facilitate ORR with its high stability and superior electro-catalytic activities^{3,30}. Like as Pt, Iridium (Ir) and Ruthenium (Ru) are the best

catalysts to great OER because of high electro-catalytic activities³¹. To apply for bi-functional catalysts, these novel metals synthesized as an alloy form, show great performance with high cost and not abundance to commercialize.

B. Transition metals

Transition metals include different oxide groups such as single metal oxides and mixed metal oxides. These transition metals are used for alternative materials of novel metals with strong points of high abundance, low cost, easy preparation, environmental friendliness and so on. Its elements have multi valences to make various types of oxide with different crystal structure, and its different crystal structure brings diverse performance. Well known transition metal oxides for bi-functional catalysts are manganese oxide (MnO_x)³², cobalt oxide (CoO_x) and nickel oxide (NiO_x)³³⁻³⁵.

C. Carbon materials

Most carbon materials usually show low catalytic activities for ORR and OER in aqueous solutions, but it show higher activities in non-aqueous solution. When the carbon materials have a nanostructure, it shows pretty higher catalytic activities with high conductivities and surface area^{36,37}. The nanostructure carbon includes different dimensional materials as one-dimensional nanotubes and nanofibers, two-dimensional graphite and graphene nanosheets, and three-dimensional nanoporous architectures. Because of its different characteristic, carbon is used as supporting material to improve the catalytic activities³⁸.

D. Metal oxide hybrid and doped materials

The low conductivity and serious aggregation of particles in metal oxide are the important drawbacks that limit its activity for ORR and OER. To overcome this limitation, well dispersion of particles is promising technique. Cho et al. have reported the considerable way to import the electrochemical activity of manganese oxide by forming composites with conductive substrates as carbon nanotubes (CNTs) and reduced graphene oxide (rGO)³⁹. Conductive substrates make a well dispersion of manganese oxide particles and overcome the limitation of low electrical conductivity.

Another way is to use dopant materials such as nitrogen (N) in the carbon framework to improve the

activity. It is the promising method which has gained increasing attention because of high catalytic activity with utilization of abundant and low cost of precursors. With replacing the atomic sites, it increases the resistance of corrosion and the performance of catalysts⁴⁰⁻⁴³.

There are various types of materials for bi-functional catalysts with different characteristics. Before making and choosing the materials, to consider the electrolyte and other conditions has to be the first. It is also important what reactions can be occurred at the surface of catalyst by its ORR and OER mechanisms.

1.3.2. ORR & OER studies

Oxygen (O₂) is the most abundant element in the Earth's crust. So, the conversion of O₂ is promising technology in these days. Its conversion is divided into two parts; one reaction is oxygen reduction reaction (ORR), and other reaction is oxygen evolution reaction (OER).

A. Oxygen reduction reaction (ORR)

The oxygen reduction reaction (ORR) is the most important reaction in life process such as not only metal-air battery but also biological respiration and fuel cells. The ORR in aqueous solutions occurs mainly by two pathways:

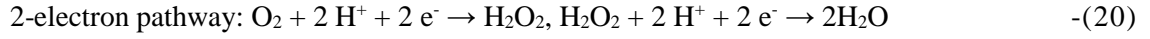
The direct four-electron reduction pathway from O₂ to H₂O, and the two-electron reduction pathway from O₂ to hydrogen peroxide (H₂O₂)^{44,45}.

In non-aqueous solutions and alkaline solutions, one-electron reduction pathway from O₂ to superoxide (O₂⁻) can also occur^{44,45}.

These reactions are written as:

- In acidic aqueous solution

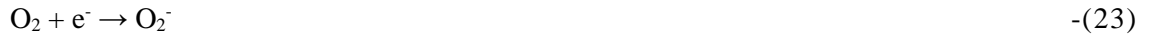




- In alkaline aqueous solution



- In non-aqueous solvents



Depending on the applications, the reduction pathways can be selected. And, these reactions also depend on the materials such as carbon. In case of carbon materials, it has some electrocatalytic activity towards ORR in alkaline solution itself. And, ORR activities and mechanisms are different depending on the types of carbon. Here is an example of graphite and glassy carbon which is used in electrochemical characterization of this work⁶⁷. The mechanisms on glassy carbon in alkaline solution are shown in Fig 3. and written as:



The 'abs' species such as $O_{2,abs}$ are absorbed on the surface of glassy carbon electrode. In this mechanism, the third process; $[O_{2,abs}]^- \rightarrow O_{2,abs}^-$ is the most important. The left one is related to inert form adsorbed on inert carbon sites, but right one that is same species migrates to an active site with following the reaction. It means this step can determine the reaction rates. Taylor et al. reported the reaction rate with its mechanism and they found that reaction rate depends on $pH^{68,69}$. Above mechanisms are occurred in alkaline solution, and its third steps only affects on rate of reaction at $pH > 10$.

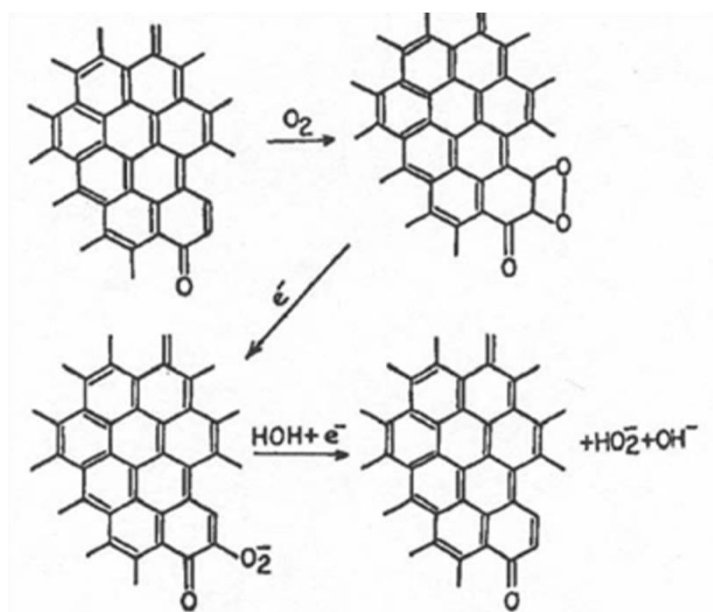


Fig. 3. The mechanism of ORR on carbon surface

B. OER studies

The oxygen evolution reaction (OER) comes from water oxidation and it is an enabler of several technological applications⁴⁶. In energy storage, it includes regenerative fuel cells, electrolyzers, solar driven water-splitting devices and metal-air batteries. OER has a large overpotential compare to ORR, and the aim of OER is to achieve the lower overpotential. Other aim of OER is to find out alternative materials for replacement of Ir and Ru oxides. Ir and Ru oxides are the best materials for OER, but they have limitations, such as high cost and scarcity^{15,13}. Among many materials, transition metal oxide such as Ni, Co, Mn oxides are possible alternative candidates with low cost, high abundance, good

conductivity, stability in alkaline solution and high electrocatalytic activity for OER. With new materials, there is a considerable point to commercialize for bi-functional catalyst⁴⁷⁻⁴⁹. The efficiency of OER is considered by relation of OER on solar fuels. That is why above mention, OER comes from water oxidation by solar energy and it can be explained with Fig 4.

In the area of solar fuels, the energy of solar radiation is utilized to drive redox reactions for the synthesis of fuels. For example:



For large scale solar fuel synthesis, it has been suggested that water oxidation is the ideal source of the protons and electrons needed for the fuel-synthesis reaction above, as water is inexpensive and abundant^{4,30}.



The challenge is to minimize the overpotentials required to drive these redox reactions such as the development of improved catalysts. One reason why the OER catalyst metric of the E(V) required to reach 10 mAcm⁻² of water oxidation is that this current density roughly matches the solar spectrum for a 10 % efficient solar to fuel device. The details of calculations to arrive this value is as follows:

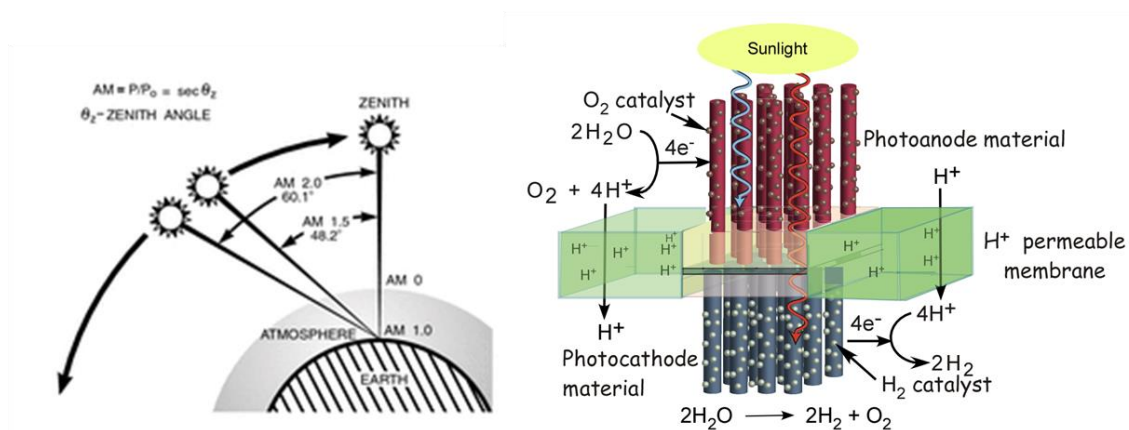


Fig. 4. The mechanism of OER comes from water oxidation by solar energy³⁰

a) In a collaborative effort, the photovoltaics industry defined the standard terrestrial solar spectrum: AM 1.5 G⁴⁶. Integration of this spectrum yields a value of $1000 \text{ Wm}^{-2} = 100 \text{ mWm}^{-2}$, an illumination intensity which is typically referred to as “1 sun”⁵⁰

b) Note that the redox potentials above for fuel synthesis and water oxidation are approximately 1.23V apart. If $1 \text{ sun} = 100 \text{ mWcm}^{-2} = 100 \text{ (mAV)cm}^{-2}$, then a 100 % efficient solar to fuel device would draw $(100 \text{ (mAV)cm}^{-2})/(1.23 \text{ V}) = 83 \text{ mAcm}^{-2}$ under AM 1.5 G^{46,50}.

c) A 10 % efficient solar to fuel device would draw 1/10th the current, at 8.3 mAcm^{-2}

d) Thus, the voltage required to drive water oxidation at 10 mAcm^{-2} is a relevant value in ranking OER catalysts for a 10 % solar to fuel device under AM 1.5 G illumination. The lower this voltage, the better the catalyst is for this application⁵¹.

The goal to meet the qualification for OER, the catalyst has to show 10 mAcm^{-2} of electrochemical activity.

1.4. Theoretical background

1.4.1. Concept of doping

Doping is usually used for semiconductor. It intentionally introduces impurities into an extremely pure, also referred to as intrinsic, material for the purpose of modulating its electrical properties. The concept of doping is useful method to improve the efficiency of catalyst by changing its electrical properties. With doping, catalysts show higher electrical activities for ORR and OER.

Doping can be explained easily by aspect of semiconductor, and it means that can be described by band theory⁷⁰. Doping a semiconductor crystal introduces allowed energy states within the band gap, but very close to the energy band that corresponds to the dopant type⁷¹. It means that donor impurities create states near the conduction band while acceptors create states near the valence band as shown in

Fig 5. The gap between these energy states and the nearest energy band is usually referred to as dopant-site bonding energy and is relatively small.

And the common dopants are categorized by periodic table groups in acceptors and donors. For example, the most common dopants are acceptors from group three and donors from group five elements⁷⁰. Boron (B), phosphorous (P) and nitrogen (N) are used to dope not only silicon in semiconductor but also carbon materials in fuel cells and metal-air batteries. By doping materials with group five elements such as phosphorus, extra valence electrons are added that become unbounded from individual atoms and allow the compound to be an electrically conductive n-type material. Doping with group three elements, which are missing the fourth valence electron, creates holes in the material lattice that are free to move. The result is an electrically conductive p-type material⁷⁰⁻⁷². In other words, a group five element is acted as an electron donor, and a group three element as an acceptor. This concept controls the electrical properties of catalysts.

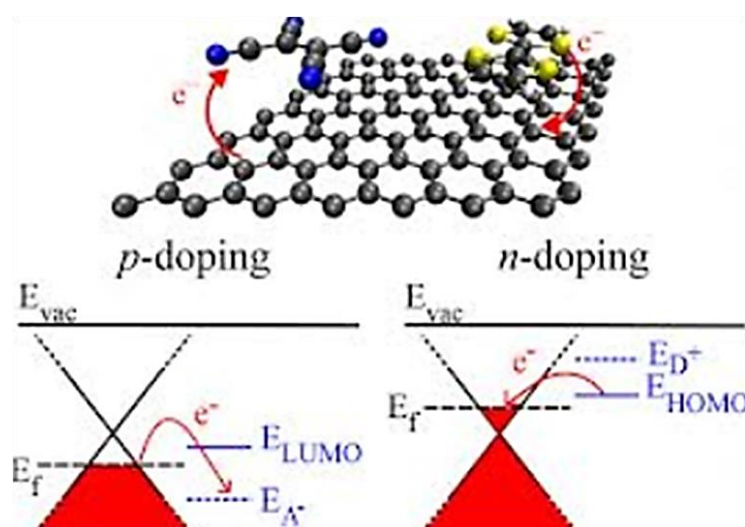


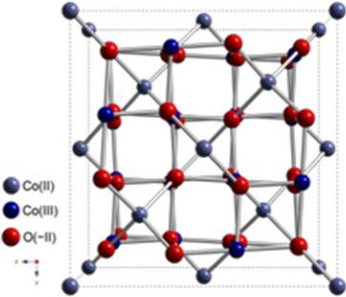
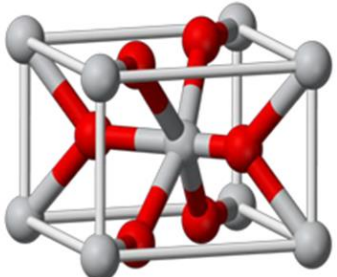
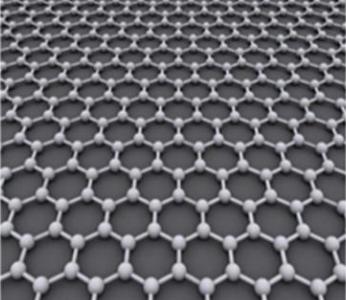
Fig. 5. Different types of doping structure explained by energy band

1.4.2. Characteristics of materials

To make a better bi-functional catalyst for ORR and OER, various types of materials have been

researched. Among materials, cobalt (Co), manganese (Mn), nitrogen (N) and reduced graphene (rGO) were used. The characteristics of main materials such as cobalt oxide, manganese oxide and graphene are shown in Table 1^{5-8,52-54}.

Table 1. Basic properties of cobalt oxide, manganese oxide and graphene

	<p style="text-align: center;">Co₃O₄ (Cobalt oxide)</p> <ul style="list-style-type: none"> ▶ It is currently utilized in the process of artificial photosynthesis -Molar Mass : 240,80g/mol -Appearance : black solid -Density : 6,11g/cm³ -Melting point : 895°C -Boiling point : 900°C (decomposes) -Solubility in water : Insoluble -Solubility : soluble in acids and alkalis
	<p style="text-align: center;">MnO₂ (Manganese oxide)</p> <ul style="list-style-type: none"> ▶ It has a wide range of applications and the most stable manganese oxide with excellent physical and chemical properties under ambient conditions. -Molar Mass : 86,9368g/mol -Appearance : brown-black solid -Density : 5,026g/cm³ -Melting point : 535°C -Solubility in water : Insoluble
	<p style="text-align: center;">Graphene</p> <ul style="list-style-type: none"> ▶ It is an atomic-scale honeycomb lattice made of carbon atoms. ▶ Due to the extremely high surface area to mass ratio of graphene, one potential application is in the conductive plates of ultracapacitors.

1.5. Objectives of work

Finding new energy materials has become increasingly important. As already mentioned, metal-air

batteries have many advantages and much research has been carried out to overcome their drawbacks. Metal-air batteries operate mainly in alkaline electrolyte, so a transition metal such as cobalt oxide is used as bi-functional catalyst because of its stability in alkaline condition. By using cobalt materials, the increased efficiency of electrochemical activity is solved by doping and using supporting materials. Doped with nitrogen and manganese, its electrochemical properties can be changed and it shows higher performance in ORR and OER. Also, catalytic materials can be dispersed well on the supporting material such as reduced graphene oxide, similar to graphene, and it has better activity because of high conductivity and surface area.

In this study, three materials for bi-functional catalysts are synthesized and compared with diverse characterization. We compare the performance of catalysts and the mechanism of OER by using different states of cobalt oxide.

II . EXPERIMENTAL

2.1. Chemicals

Graphite, sulfuric acid (H_2SO_4 , 95 – 98 %), potassium permanganate ($\text{KMnO}_4 \geq 99.3$ %) and tetraphenylphosphonium tetraphenylborate (TPPTPB) were obtained from Aldrich. Potassium persulfate ($\text{K}_2\text{S}_2\text{O}_8$, 99 %) and phosphorous pentoxide powder ($\text{P}_2\text{O}_5 \geq 98.0$ %) were obtained from Kanto chemicals. Sodium chloride ($\text{NaCl} \geq 99.0$ %) and ammonium hydroxide (NH_4OH , 28.0%) were obtained from Daejung. Hydrogen peroxide ($\text{H}_2\text{O}_2 \geq 34.5$ %) was purchased by Samchun. Cobalt acetate ($\text{Co}(\text{Ac})_2$) and manganese acetate ($\text{Mn}(\text{Ac})_2$) were obtained by Alfa aesor.

2.2. Synthesis of Graphene oxide

Graphene oxide (GO) was synthesized by modified Hummer's method using graphite powder and oxidizing agent⁵⁵. One gram of graphite powder was grinded with 50 g of sodium chloride to make the fine power. Afterwards, it was washed by DI water 5~10 times to remove sodium chloride and the ethanol is used for final wash. The remaining graphite was dried in a vacuum oven at 60 °C for 1 hour. The dried powder was transferred to a round bottom flask, and 4 mL of sulfuric acid was added with 0.84 g of $\text{K}_2\text{S}_2\text{O}_8$ and 0.84 g of P_2O_5 . The mixture was stirred at 80 °C for 4.5 h. It was cooled for 10~20 minutes and 167 mL of DI water was added. It was stirred overnight at room temperature. Afterwards, the mixture was washed by DI water 5~10 times and the ethanol was used for final wash, and dried in vacuum oven at 60 °C for 1 h. The collected powder was transferred in the two-necked round flask in an ice bath with 40 mL of H_2SO_4 . Five grams of KMnO_4 was added with slow stirring until the contents were completely dissolved. Then, 84 mL of DI water was added into the mixture and it was stirred at 35 °C for 2 h. For final step, 167 mL of DI water and 10 mL of H_2O_2 were added slowly in an ice bath

with stirring for 30 min. The resulting mixture was washed with DI water and ethanol until pH 7, and then dark brown powder was collected after drying in a vacuum oven at 60 °C for overnight.

2.3. Synthesis of catalysts

2.3.1. Preparation of cobalt oxide with reduced graphene oxide (rGO)

Graphene oxide (GO) was prepared by adopting by modified Hummer's method. The GO was dispersed in the ethanol at a 0.03 g/L of concentration with ultrasonication. Cobalt (II) acetate ($\text{Co}(\text{Ac})_2$) was prepared as a solution for 0.2 M of concentration. The amount of 250 mL of GO/ethanol solution was mixed with 5 mL of 0.2 M $\text{Co}(\text{Ac})_2$ solution and 5 mL of DI water. The mixture was stirred at 80 °C for 10 h. After stirring, the mixture was transferred to teflon container to use for hydrothermal reaction^{56,57}. The mixture was heated until 150 °C by 5 °C/min of heating rate, and the reaction was kept for 3 h in an autoclave. Afterwards, the mixture was washed by DI water until pH 7, and ethanol was used for final wash. The resulting cobalt oxide-reduced graphene oxide hybrid was collected after drying in vacuum oven at 50 °C for overnight.

2.3.2. Preparation of manganese doped cobalt oxide with rGO

To prepare manganese doped catalyst, it followed the same method to prepare cobalt oxide with rGO sample. Before chemical heating process, the amount of $\text{Co}(\text{Ac})_2$ solution was changed. Manganese acetate ($\text{Mn}(\text{Ac})_2$) was prepared 0.2 M concentration of solution. With 250 mL of GO/ethanol solution and 5 mL of DI water, 3.75 mL of $\text{Co}(\text{Ac})_2$ solution and 1.25 mL of $\text{Mn}(\text{Ac})_2$ solutions were added. Afterwards, followed processes were same.

2.3.3. Preparation of cobalt oxide with nitrogen doped rGO (NrGO)

To doped nitrogen in rGO, the amount of DI water was changed. Ammonium hydroxide (NH_4OH) was used as precursor for nitrogen doped, and it was added the amount of 1.25 mL with 3.75 mL of DI

water. Like Manganese doped catalyst, other processes were same.

2.3.4. Preparation of cobalt hydroxide.

Cobalt hydroxide was prepared to demonstrate the mechanism of OER. When the mechanism of OER was explained, cobalt oxide and cobalt hydroxide were synthesized with adding tetraphenylphosphonium tetraphenylborate (TPPTPB). TPPTPB has many conductive carbon groups and has difficulty in removing boron and phosphorous, so it makes catalysts have high conductivity of carbon without change of other characteristics. Cobalt hydroxide-reduced graphene oxide hybrid ($\text{Co(OH)}_2/\text{rGO}$) was synthesized by 5 mL of 0.2 M of Co(Ac)_2 , 250 mL of GO/ethanol, 1.25 mL of TPPTPB and 3.75 mL of DI water. It underwent chemical heating process at 80 °C for 10 h with stirring. Afterwards, the mixture was washed by DI water until pH 7, and ethanol was used for final wash. The resulting cobalt hydroxide and rGO hybrid was collected after drying in vacuum oven at 50 °C for overnight. Cobalt oxide and rGO hybrid was collected through hydrothermal reaction with autoclave. The mixture was heated until 150 °C by 5 °C/min of heating rate, and the reaction was kept for 3 h in an autoclave. Then, it also washed and dried with same conditions of cobalt hydroxide. These two catalysts were used for explain the mechanism of OER with higher performance.

2.4. Characterization

2.4.1. Morphological analysis

The morphologies and size distribution of all hybrid catalysts were measured by scanning electron microscope (SEM, S-4800, Hitachi) and field emission-transmission electron microscopy (FE-TEM, HF-3300/NB5000/S-4800, Hitachi). SEM samples were prepared by drop-coating the samples onto carbon tape and TEM samples were prepared by drop-drying the samples from their diluted solution as all catalysts in IPA onto carbon grids.

Structure studies of all catalysts were carried out by X-ray diffraction (XRD, Miniflex 600, Rigaku). The diffraction patterns of hybrid catalysts were obtained in 2θ ranges from 5 to 70°. The clean powder

samples were directly place on XRD sample holder and the scan were carried out with a step size of 0.020.

2.4.2. Elemental analysis

The reactivity of given atoms could be modified by hybrid, and all catalysts had different electronic characteristic. For these reasons, surface elemental composition and the oxidation state of cobalt hybrid catalysts were investigated by analysis of the X-ray photoelectron spectra (XPS, Theta probe AR-XPS system, Thermo fisher scientific (U.K)). XPS data were obtained from a monochromated Al K α source ($h\nu = 1486.6$ eV). In addition it was operated at 150 W with 15 kv of X-ray energy.

2.4.3. Electrochemical studies

Electrochemical activities were performed on a Biologic potentiostat/galvanic with a three-electrode cell configuration using platinum (Pt) wire, Ag/AgCl saturated electrode, and glassy carbon (3 mm, ϕ) as counter, reference and working electrodes, respectively.

The catalyst ink was prepared to coat onto a polished glassy carbon (GC) electrode. Five mg of catalyst powder was dispersed in 187 μ L of DI water, 63 μ L of isopropyl alcohol (IPA) and 4 μ L of nafion solution (5 wt.%, Aldrich) by ultra sonication for 30 min. 3.7 μ L of suspended catalyst ink was dropped onto GC electrode and dried in room temp.

The oxygen reduction reaction (ORR) and oxygen evolution reaction (OER) activities were carried out with rotating disk electrode (RDE) in 0.1 M KOH electrolyte at a 5 mVs⁻¹ of scan rate.

III. RESULTS & DISCUSSION

PART 1: Studies of catalysts with different doping

3.1. Morphology studies of catalysts

The particle sizes and distribution of three catalysts were observed differently by TEM images by Fig 6. It can be seen from the images that different particle sizes were observed. Cobalt oxide with reduced graphene oxide ($\text{Co}_3\text{O}_4/\text{rGO}$) was formed around 20 nm as a size with square types.

Compare to $\text{Co}_3\text{O}_4/\text{rGO}$, manganese doped catalysts ($\text{MnCo}_2\text{O}_4/\text{rGO}$) was shown much smaller size less than 10 nm. By two images, particle size was affected by doping of manganese. By comparison of $\text{Co}_3\text{O}_4/\text{rGO}$ and Co_3O_4 with nitrogen doped rGO ($\text{Co}_3\text{O}_4/\text{NrGO}$), different dispersion state of cobalt oxide on graphene sheet was observed. Sizes of particles were not much different, but dispersion was better with nitrogen doping.

3.2. Structural studies of catalysts

Three catalysts showed similar X-ray diffraction (XRD) peaks as a spinel structure (AB_2O_4 , A,B = transition metal) in Fig. 7. The interesting issue of spinel structure is caused by its physicochemical properties which are greatly sensitive to the composition, structure parameters, and distribution and oxidation state of cations such as Co^{2+} and Co^{3+} .

The formation of $\text{Co}_3\text{O}_4/\text{rGO}$ was confirmed by the 2-theta value of 31° , 36.5° , 44.4° , 58.7° and 64.6° as Co_3O_4 spinel structure⁵¹, and MnCo_2O_4 was known by the 2-theta value of 55° as Mn peak with doping^{28,56}. $\text{Co}_3\text{O}_4/\text{NrGO}$ was not much different from $\text{Co}_3\text{O}_4/\text{rGO}$ due to any change of metal composition.

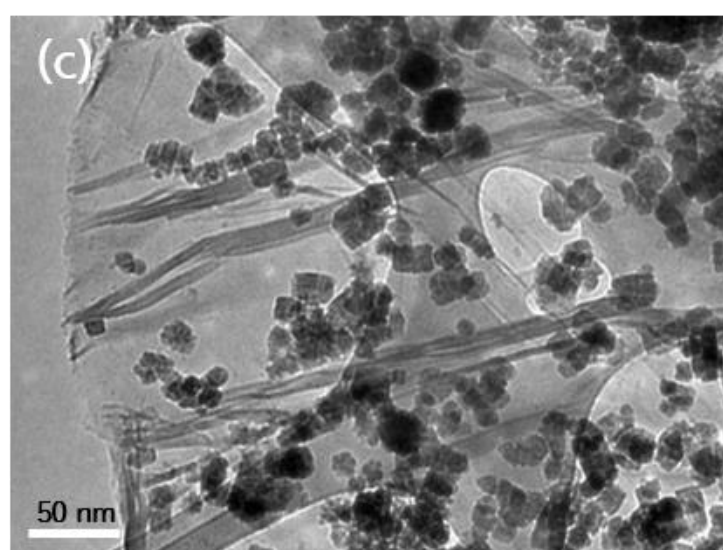
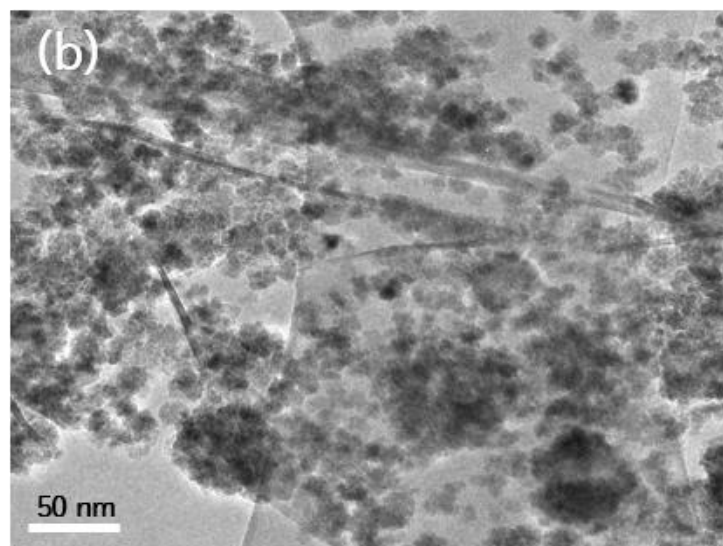
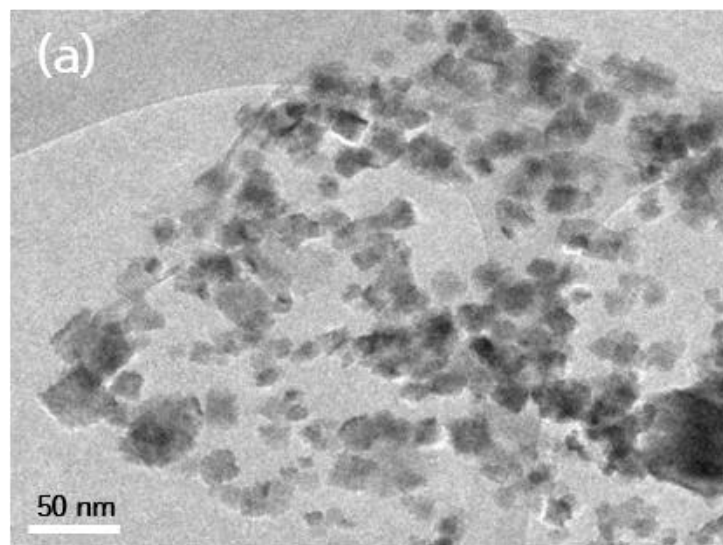


Fig. 6. TEM images of (a) $\text{Co}_3\text{O}_4/\text{rGO}$, (b) $\text{MnCO}_2\text{O}_4/\text{rGO}$ and (c) $\text{Co}_3\text{O}_4/\text{NrGO}$

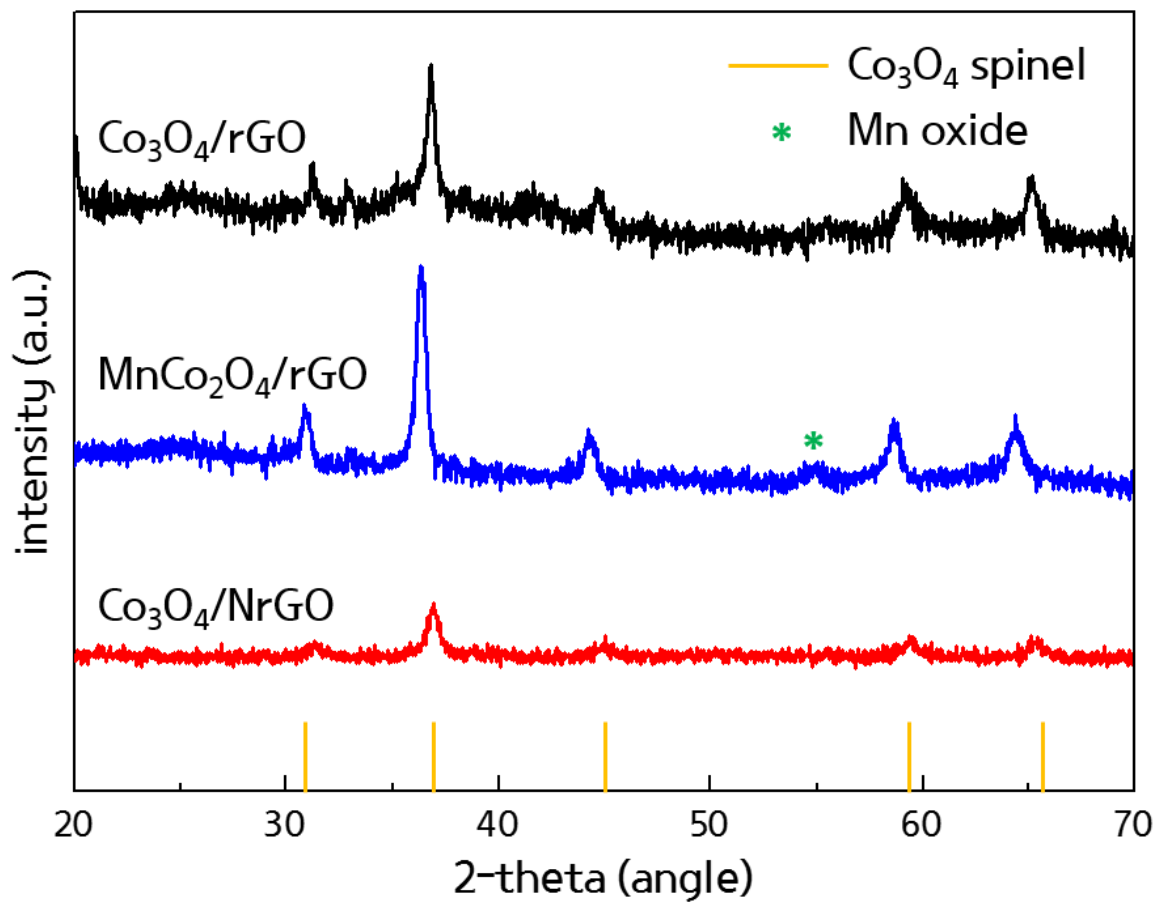


Fig. 7. XRD patterns of the $\text{Co}_3\text{O}_4/\text{rGO}$, $\text{MnCo}_2\text{O}_4/\text{rGO}$ and $\text{Co}_3\text{O}_4/\text{NrGO}$

3.3. Chemical and electronic properties of catalysts

The electronic structures of three catalysts were examined by X-ray photoelectron spectroscopy (XPS). The wide XPS survey spectra showed the presence of Co, O and C in all of catalysts as shown in Fig 8. The peak of Mn was observed in MnCO_2/O_4 and that of N was observed in $\text{Co}_3\text{O}_4/\text{NrGO}$. More deeply, high resolution analysis was shown in Fig 9. In Co 2p spectra of $\text{Co}_3\text{O}_4/\text{rGO}$ confirmed the oxidation state of Co as Co^{2+} and Co^{3+} ⁵⁷. With doping, the peaks of Co^{2+} and Co^{3+} were negative shifted. $\text{MnCO}_2/\text{O}_4/\text{rGO}$ was shown the value of binding energy as 643 eV and 655 eV with tendency of Mn^{2+} and Mn^{3+} ⁵⁸. These peaks ensured the formation of spinel structure which includes different oxidation states of cations in one structure. As N was doped on rGO sheets, the peaks revealed as pyridinic and pyrrolic N species in high resolution XPS spectra^{59,60}. Higher electronegativity N (3.04 V) than C (2.55 V) made positively charge state. Especially, pyridinic N formed resonance state. It made more electron transfer in structure, and it enhanced the higher electrochemical activities.

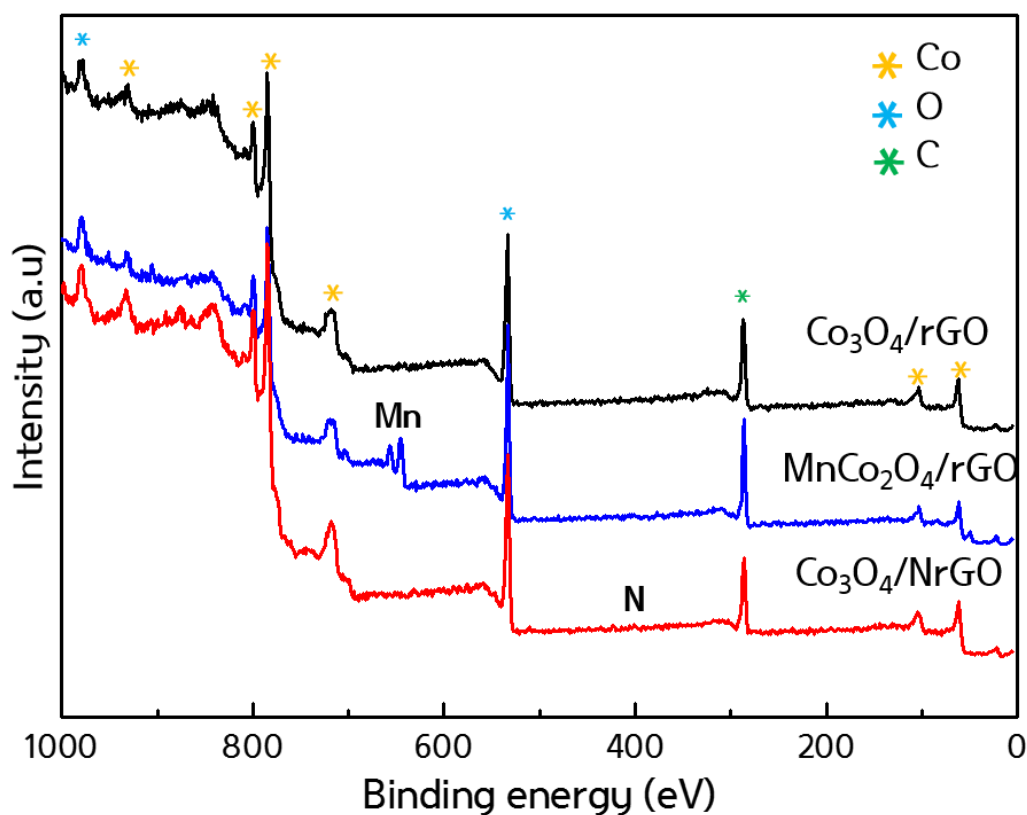


Fig. 8. XPS survey spectra of $\text{Co}_3\text{O}_4/\text{rGO}$, $\text{MnCO}_2/\text{O}_4/\text{rGO}$ and $\text{Co}_3\text{O}_4/\text{NrGO}$

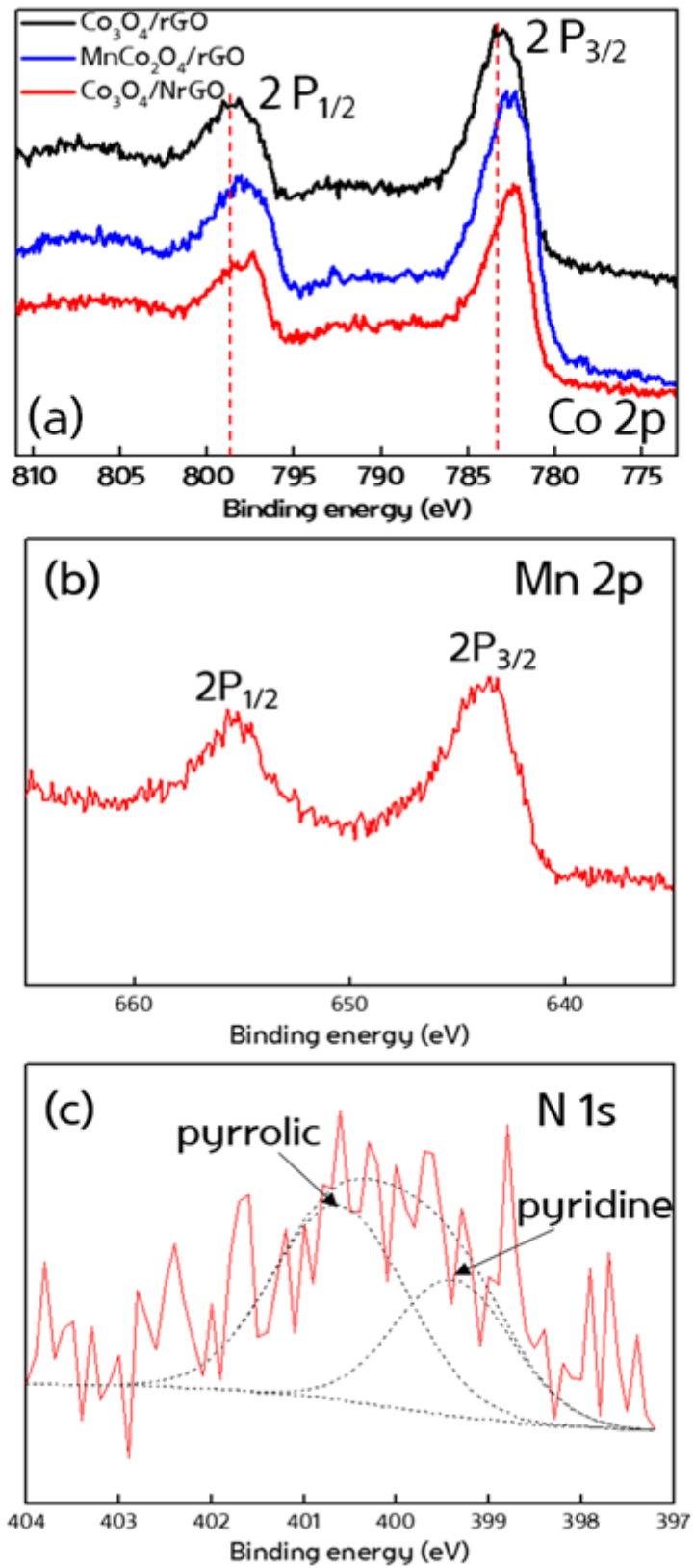


Fig. 9. (a) Co 2p spectra of $\text{Co}_3\text{O}_4/\text{rGO}$, (b) Mn 2p spectra of $\text{MnCo}_2\text{O}_4/\text{rGO}$ and (c) N 1s spectra of $\text{Co}_3\text{O}_4/\text{NrGO}$

3.4. Electrochemical activities of catalysts

3.4.1. Oxygen reduction reaction activities

The ORR catalytic activities of three catalysts were measured by rotating disk electrode (RDE) in a 0.1 M KOH electrolyte. Three catalysts were loaded on glassy carbon electrode, and these different rotating speed (rpm) of electrode was used in O₂-saturated and N₂-saturated conditions. The ORR activities trace and Koutecky-Levich plot of three catalysts were illustrated in Fig 10. All catalysts showed charge transfer from the onset potential region around 0.85 V – 0.99 V vs.RHE. The ORR for all of catalysts revealed mixed diffusion-kinetic control in the potential region little different such as 0.5 V – 0.85 V of Co₃O₄/rGO and MnCo₂O₄/rGO and 0.7 V – 0.85 V of Co₃O₄/NrGO. From 0.35 V vs.RHE to mixed potential region was diffusion limiting current region. It means that the ORR of all catalysts was diffusion controlled under this region. This limiting current density can be both increased and decreased by virtue of the rotating rate and can be controlled by mass transport rate.

The electron transfer number (n) was calculated by Koutecky-Levich equation^{61,62}:

□ Koutecky-Levich equation □

$$\frac{1}{I} = \frac{1}{I_k} + \frac{1}{I_L} = \frac{1}{I_k} + \frac{1}{B\omega^{1/2}}$$

$\omega = 2\pi N$ (N = rpm)

$$B = 0.62 nFC_bD_o^{2/3}\nu^{-1/6}$$

Where, n is the number of electrons transferred in the ORR, F is the Faraday constant (96,485 Cmol⁻¹), C_b is the bulk concentration of O₂ (1.2 x 10⁻⁶ molcm⁻³), D_o is the diffusion coefficient of O₂ (1.9 x 10⁻⁵ cm²s⁻¹), and ν is the viscosity of the electrolyte. In the case of 0.1 M KOH, ν has been reported as 0.01 cm² s⁻¹. ω indicates the angular rotation rate of the electrode. Kinetic current density (j_k) was obtained from various voltages from the ORR curve (0.3 V to 0.45 V vs.RHE), and it was plotted as a function of $\omega^{-1/2}$. K-L plots showed linearity, and it could be concluded that the ORR for two catalysts was followed a four-electron transfer reaction.

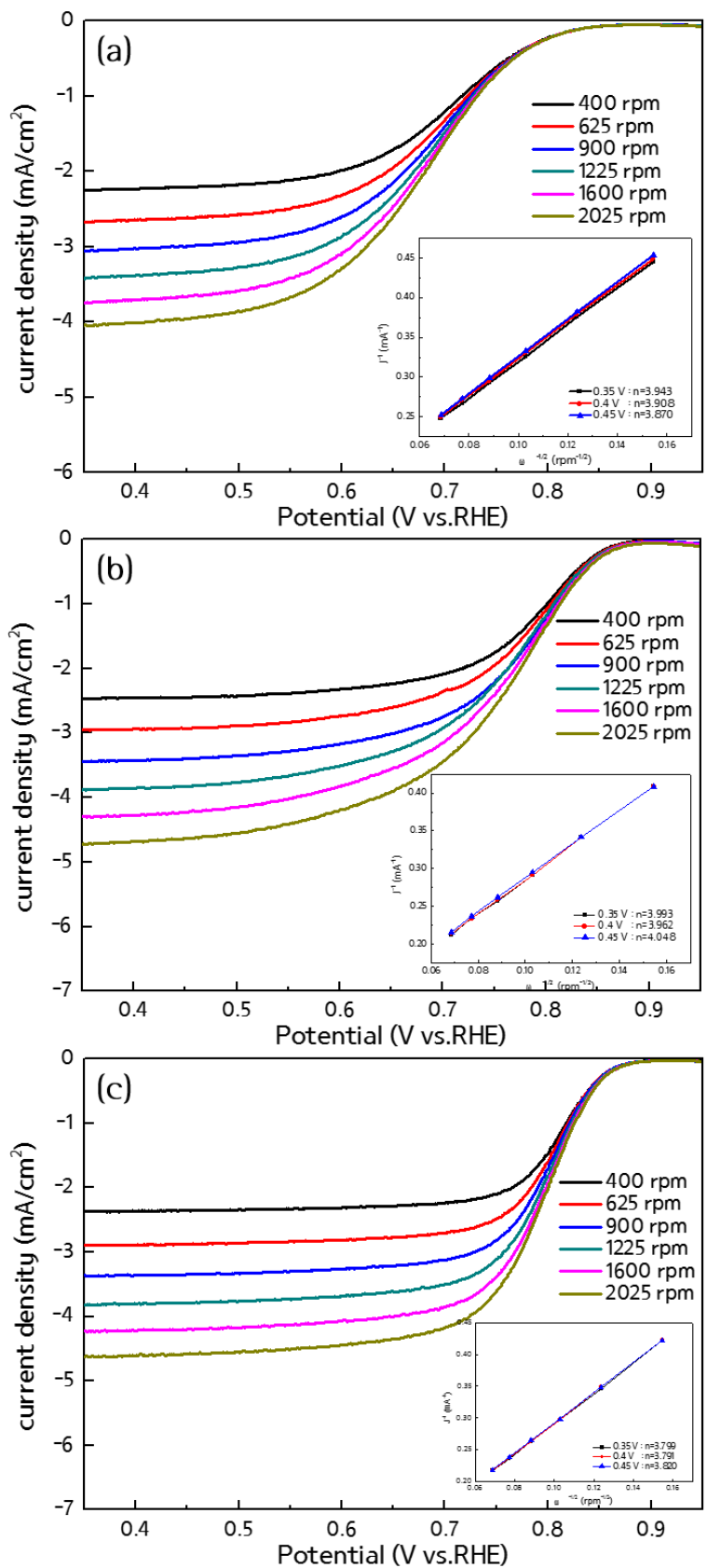


Fig. 10. RDE traces and Koutechy-Levich plot of (a) Co₃O₄/rGO, (b) MnCO₂O₄/rGO and (c) Co₃O₄/NrGO

To compare the ORR activities of all samples, RDE was carried out at a rotating rate of 1600 rpm. As shown in Fig 11, the onset potential was increased in order of $\text{Co}_3\text{O}_4/\text{rGO}$ (0.85 V), $\text{MnCo}_2\text{O}_4/\text{rGO}$ (0.89 V) and $\text{Co}_3\text{O}_4/\text{N-rGO}$ (0.9 V) at the rotation speed of 1600 rpm in 0.1 M KOH. And the order of half wave potential was same: $\text{Co}_3\text{O}_4/\text{rGO}$ (0.7 V), $\text{MnCo}_2\text{O}_4/\text{rGO}$ (0.75 V) and $\text{Co}_3\text{O}_4/\text{N-rGO}$ (0.8 V). Half wave potentials, defined as the potential at the measured current reaches the half of the limiting current. ORR activities were better with doping, and the best ORR activity was generated by nitrogen doping. Mass activities of all catalysts were evaluated with RDE curve at 0.75 V in a 0.1 M KOH. The mass activity is based on catalytic atomic % of all catalyst, and it was measured by thermal gravimetric analysis (TGA) as ~73% by mass. Despite of better ORR activity, $\text{MnCo}_2\text{O}_4/\text{rGO}$ showed lower mass activity than $\text{Co}_3\text{O}_4/\text{rGO}$. As already confirmed in TEM studies, particle size were smaller with manganese doping. It was used to explain the mass activity. It means that there were lower amount of catalytic particles with same amount. From two graphs (Fig. 11 and Fig. 12) demonstrate the order of ORR activity of catalysts was $\text{Co}_3\text{O}_4/\text{NrGO} > \text{MnCo}_2\text{O}_4/\text{rGO} > \text{Co}_3\text{O}_4/\text{rGO}$ and that of same amount was $\text{Co}_3\text{O}_4/\text{NrGO} > \text{Co}_3\text{O}_4/\text{rGO} > \text{MnCo}_2\text{O}_4/\text{rGO}$.

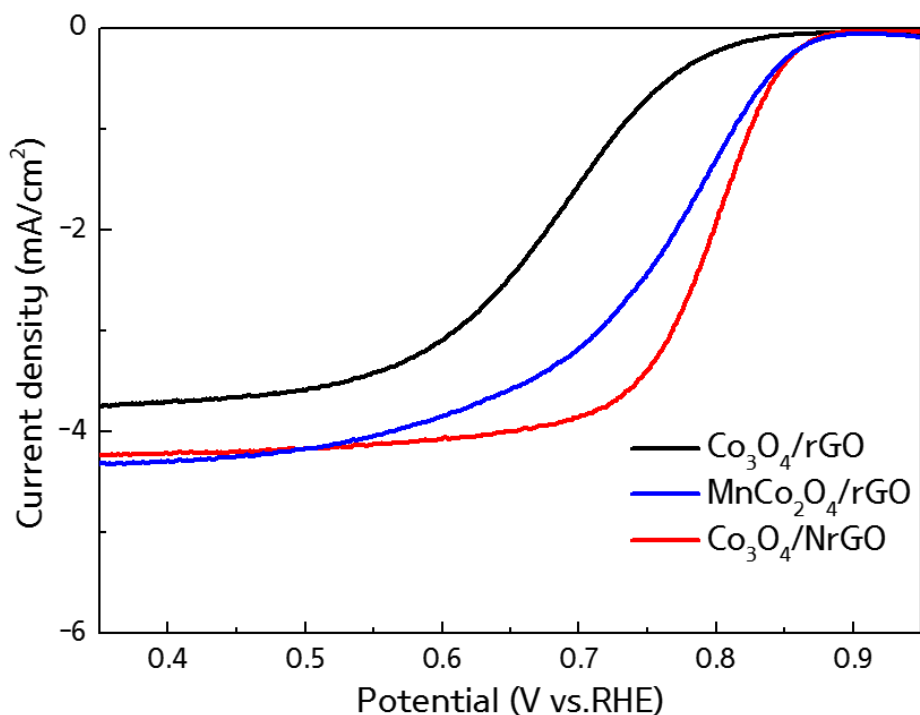


Fig. 11. ORR comparison of $\text{Co}_3\text{O}_4/\text{rGO}$, $\text{MnCo}_2\text{O}_4/\text{rGO}$ and $\text{Co}_3\text{O}_4/\text{NrGO}$

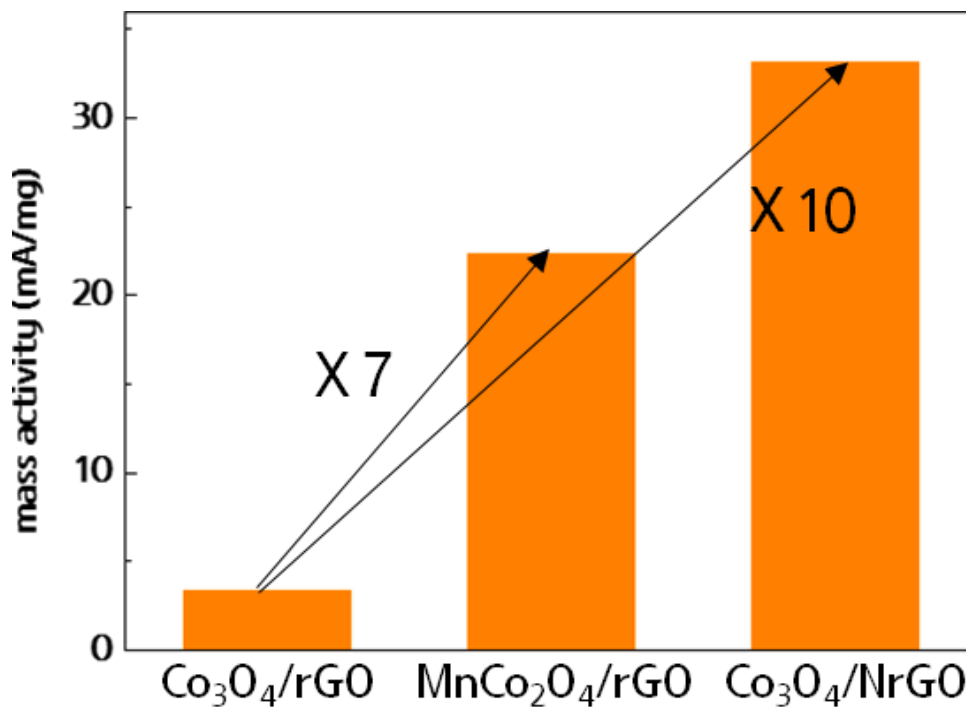
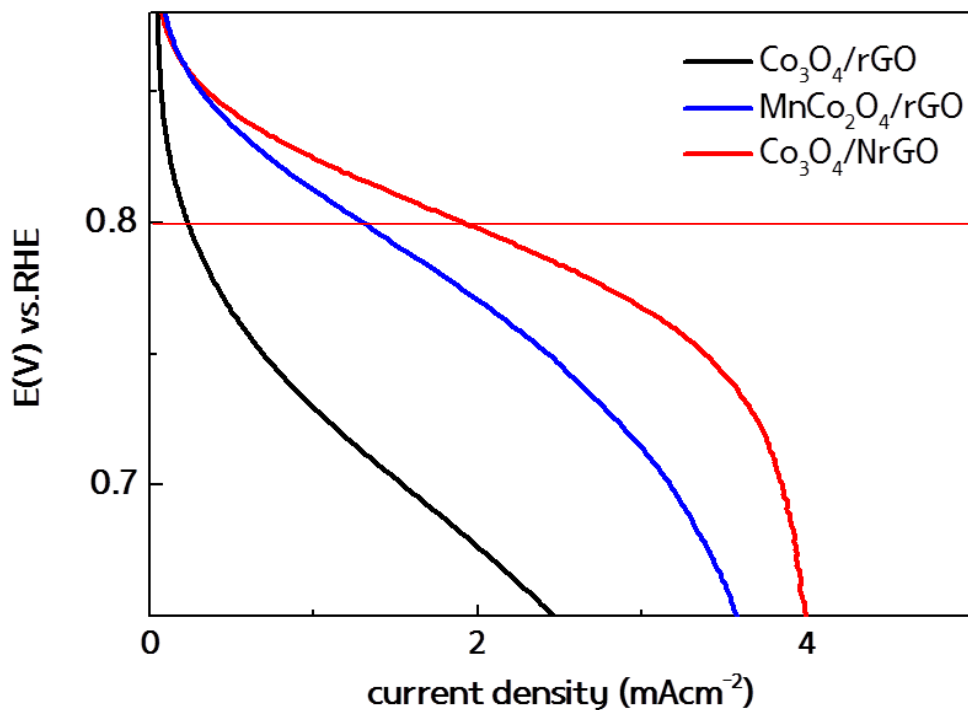


Fig. 12. Tafel plot of the three catalysts and mass activities of that at 0.8 V vs. RHE

3.4.2. Oxygen evolution reaction activities

To be satisfied with requirement of bi-functional catalyst, oxygen evolution reaction (OER) activity had to be characterized. As the ORR activity was measured, RDE technique was used with different potential range from ORR measurement. The potential was needed to more positive direction (1.0 V – 2.0 V vs.RHE), but other conditions were fixed as N₂/O₂-saturated 0.1 M KOH at 1600 rpm to compare three catalysts. The different OER activities were shown in Fig 12, and the current density of 10 mAcm⁻² was used for evaluation. The OER is mainly occurred in solar energy systems. To apply for the applications, solar cell has to show 10 % of efficiency, and it was equal 10 mAcm⁻² in electrochemical cell. From Fig 12, three catalysts followed the order of Co₃O₄/NrGO (1.62V vs.RHE), Co₃O₄/rGO (1.64 V vs.RHE) and MnCo₂O₄/rGO (1.66V vs.RHE). In ORR studies, there are evident differences by three catalysts with doping, but OER was not much affected by doping.

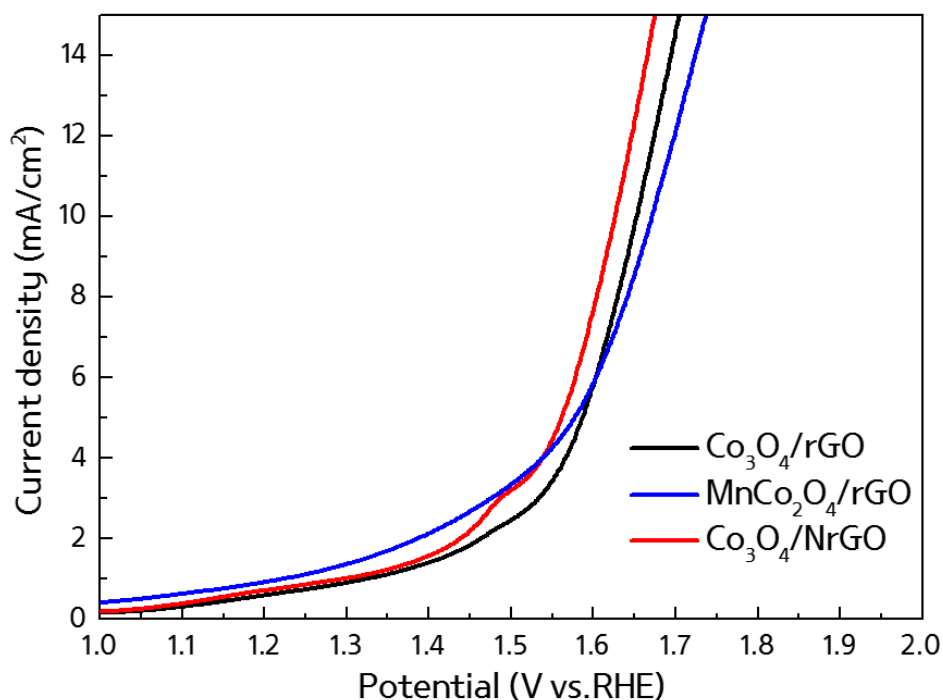


Fig. 13. OER comparison of Co₃O₄/rGO, MnCo₂O₄/rGO and Co₃O₄/NrGO

3.4.3. Evaluation for bi-functional catalysts

ORR and OER studies were discussed in 3.4.1 and 3.4.2.. Based on electrochemical activities ORR and OER, ability of bi-functional catalysts is evaluated. Bi-functional catalysts have both reactions at the same sites. The standard current density of ORR is half wave potential and that of OER is 10 mA cm^{-2} . The former value was yielded by probability for apply to electrochemical cell and the latter value was yield by probability for commercialization of solar cell. It means that bi-functional catalysts have to be enough to use as catalysts for both of electrochemical cell and solar cell. The equation of oxygen electrode potential was written as:

$$\text{Oxygen electrode } E(\text{V}): \text{OER active } E(\text{V})_{J=10 \text{ mA cm}^{-2}} - \text{ORR half-wave } E(\text{V})$$

With manganese doped, ORR activity was increased compare to $\text{Co}_3\text{O}_4/\text{rGO}$, but the OER activity was decreased opposite to ORR activity. In case of nitrogen doped catalysts, both ORR and OER activities were increased compared with $\text{Co}_3\text{O}_4/\text{rGO}$. The oxygen electrode potential as calculated based on these values. The values of $\text{Co}_3\text{O}_4/\text{rGO}$, $\text{MnCo}_2\text{O}_4/\text{rGO}$ and $\text{Co}_3\text{O}_4/\text{NrGO}$ were 0.94 V, 0.91 V and 0.82 V vs.RHE. These values were compared with Iridum oxide (IrO_2) was known as the best bifunctional catalyst showed the value of 0.92 V because of higher OER activity and the Platinum (Pt) was used for the best ORR catalyst showed the value of 1.16 V because of lower OER activity^{3,4,30}. Pure Mn oxide was already researched that has the value of 1.04 V as bifunctional catalytic activity⁶³.

PART 2: Studies the OER mechanism

3.5. Comparison of catalyst morphologies

The particle distribution of $\text{Co(OH)}_2/\text{rGO}$ and $\text{Co}_3\text{O}_4/\text{rGO}$ were observed totally different by SEM images. $\text{Co(OH)}_2/\text{rGO}$ was formed as sheet of graphene, which was difficult to distinguish whether the surface was cobalt hydroxide or graphene oxide sheet. The reason why it was not good distribution and seemed as only graphene sheet was no process of the hydrothermal reaction. Compare to $\text{Co(OH)}_2/\text{rGO}$, $\text{Co}_3\text{O}_4/\text{rGO}$ formed around 20 nm as a size which looked like a square. It was well distributed nanoparticles on graphene sheet, which the surface of GO was well dispersed with cobalt oxide nanoparticles. The TEM studies, the difference of $\text{Co(OH)}_2/\text{rGO}$ and $\text{Co}_3\text{O}_4/\text{rGO}$ was observed more certainly in Fig 15.^{4,9} On the graphene sheet, the cobalt hydroxide particle was observed and darker site was composited with cobalt hydroxide by energy dispersive spectrometer (EDS) study as shown in Fig 16. For $\text{Co}_3\text{O}_4/\text{rGO}$, it was shown the square and cubic particle around 20 nm of size as same as SEM images. The cobalt oxide particles could be distinguished easier than graphene sheet.

3.6. Comparison of catalyst structure

The morphology tendency of two catalysts was explained with crystalline structure. $\text{Co(OH)}_2/\text{rGO}$ and $\text{Co}_3\text{O}_4/\text{rGO}$ had different XRD patterns. The 2-theta value of 19° , 32.5° , 38° , 51° , 57.5° , 59.5° , 61° , 68.5° , 69.5° was shown for $\text{Co(OH)}_2/\text{rGO}$ in Fig 16a. It matched cobalt hydroxide as chemical formula as H_2CoO_2 (Co(OH)_2). From the 2-theta value of 19° , 31° , 37° , 38.5° , 44.5° , 55.5° , 59° , 65° of $\text{Co}_3\text{O}_4/\text{rGO}$ was matched with spinel $\text{Co}_{2.87}\text{O}_4$ exactly^{57,64}. Based on the XRD parameters of $\text{Co}_3\text{O}_4/\text{rGO}$, the image of spinel structure could be drawn in Fig 17b.

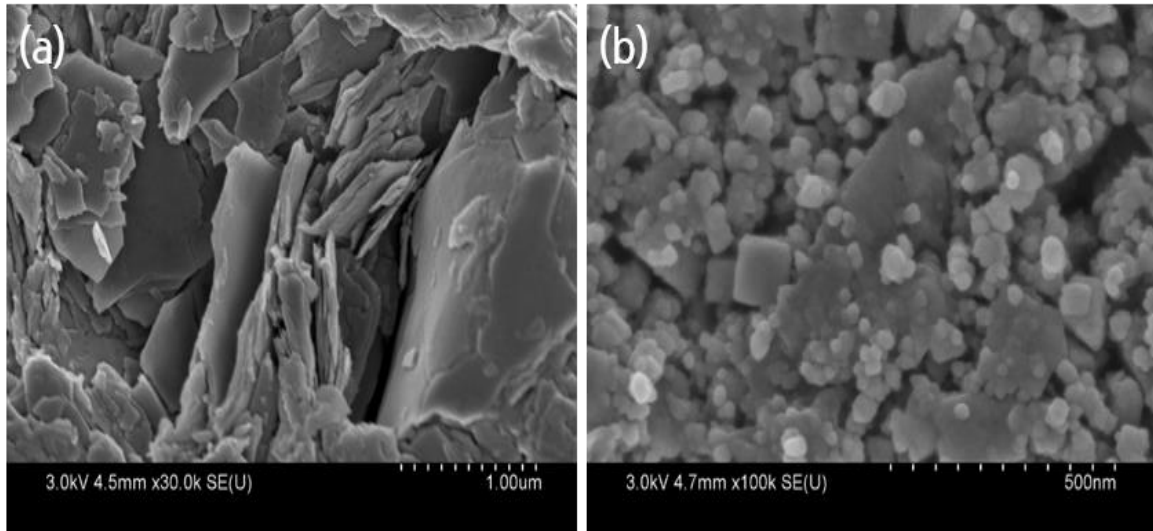


Fig. 14. SEM images of (a) Co(OH)₂/rGO and (b) Co₃O₄/rGO

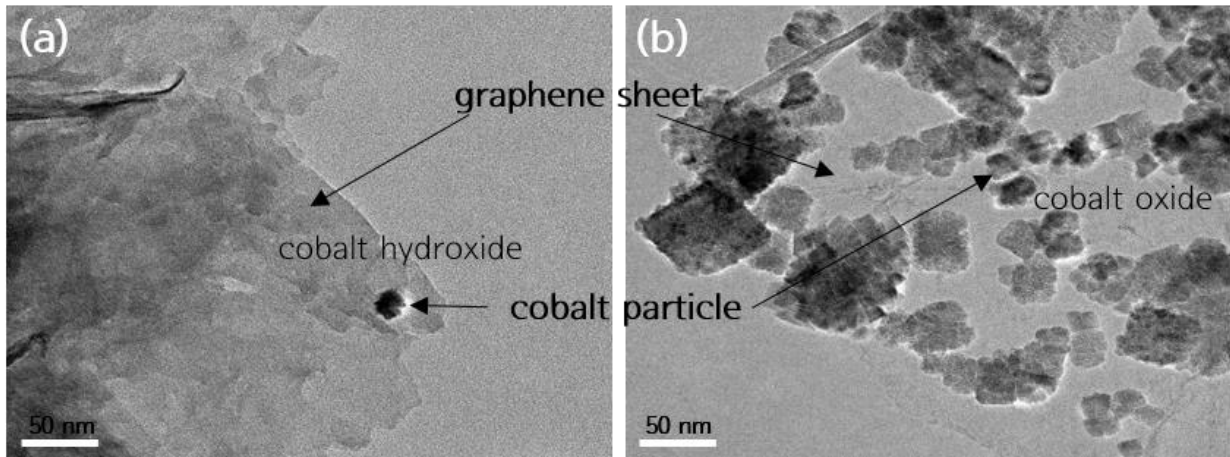


Fig.15. TEM images of (a) Co(OH)₂/rGO and (b) Co₃O₄/rGO

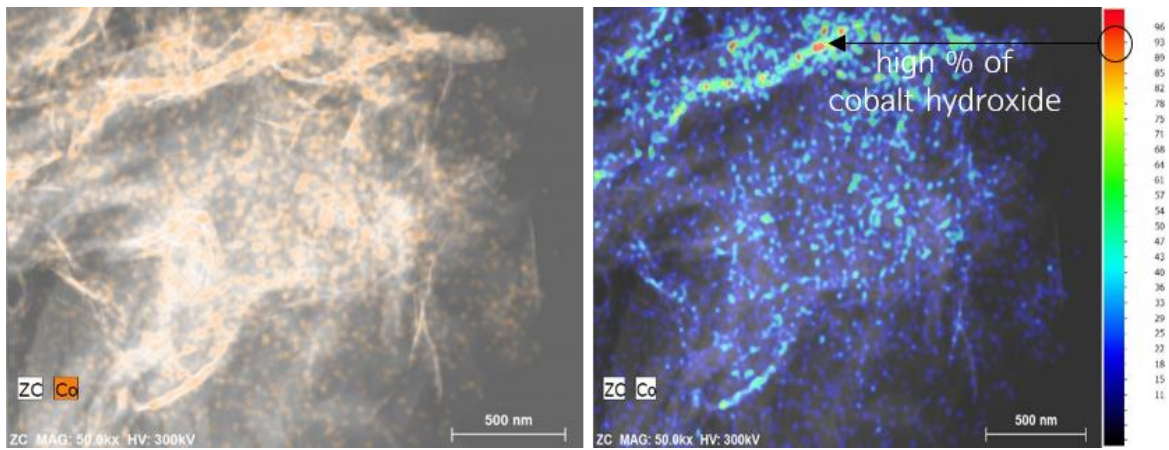
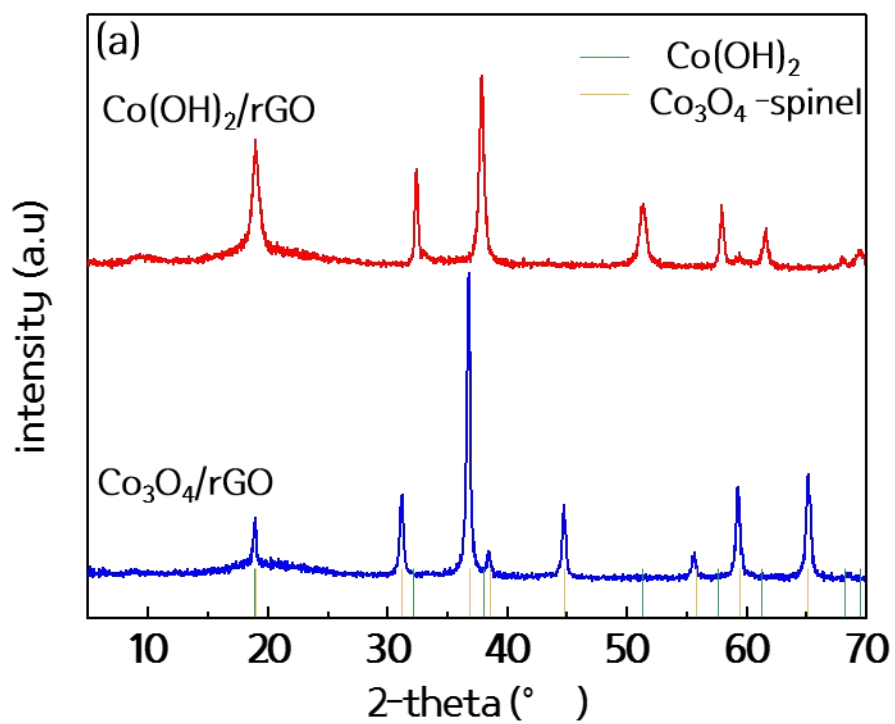


Fig. 16. EDS images of $\text{Co}(\text{OH})_2/\text{rGO}$.

The amount of Cobalt percentages of catalysts was revealed by different color.



(b) spinel structure

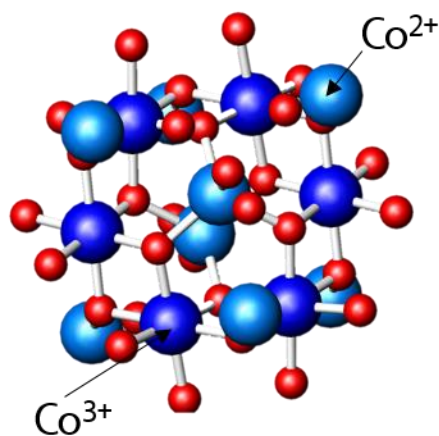


Fig. 17. (a) XRD patterns of $\text{Co(OH)}_2/\text{rGO}$ and $\text{Co}_3\text{O}_4/\text{rGO}$, (b) The structure of $\text{Co}_3\text{O}_4/\text{rGO}$ was drawn based on XRD peak values.

3.7. Comparison of chemical and electronic properties

Electronic structure of $\text{Co(OH)}_2/\text{rGO}$ and $\text{Co}_3\text{O}_4/\text{rGO}$ was examined by XPS. The wide XPS survey spectra showed the presence of Co, O and C in both of catalysts. There was only one difference in synthesis steps, and it could also be confirmed by atomic spectra. In Co 2p spectra in Fig 18a, the binding energy of 781 eV, 787 eV, 797 eV and 803.5 eV matched Co(OH)_2 ⁶⁵. Whereas, $\text{Co}_3\text{O}_4/\text{rGO}$ didn't show the peak in that of binding energy regions, but it showed Co 2p_{1/2} and Co 2p_{3/2} spectra as 796 eV and 780 eV which could be confirmed cobalt oxidation as Co^{3+} ⁵⁷. In O 1s spectra in Fig 19b, the peak positions were different in $\text{Co(OH)}_2/\text{rGO}$ and $\text{Co}_3\text{O}_4/\text{rGO}$. The 531 eV of $\text{Co(OH)}_2/\text{rGO}$ mentioned OH- bonded to Co^{2+} , 529 eV and 532 eV of $\text{Co}_3\text{O}_4/\text{rGO}$ matched metal-O and C=O bond⁶⁶.

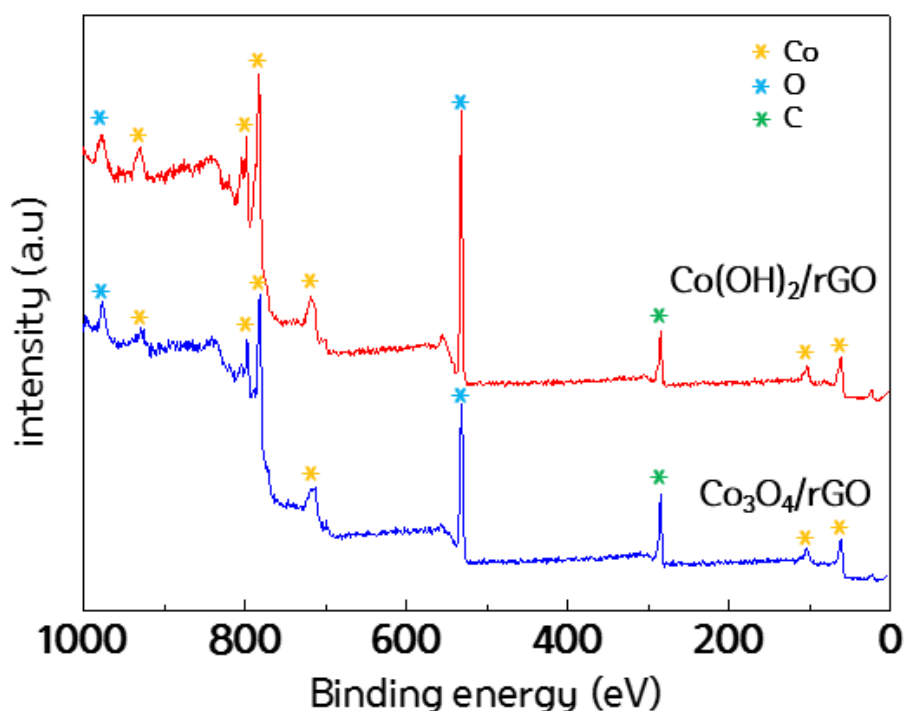


Fig. 18. XPS survey spectra of $\text{Co(OH)}_2/\text{rGO}$ and $\text{Co}_3\text{O}_4/\text{rGO}$

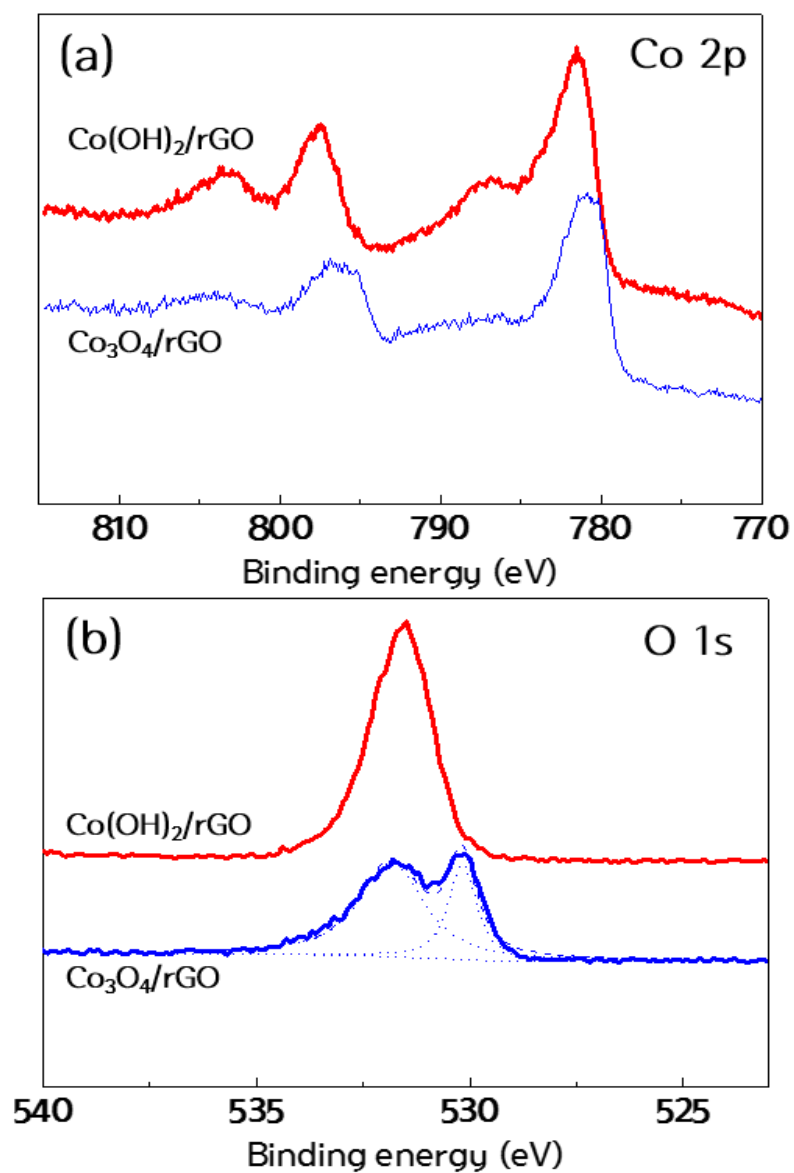


Fig. 19. (a) Co 2p and (b) O 1s XPS spectra of Co(OH)₂/rGO and Co₃O₄/rGO

3.8. Electrochemical studies

3.8.1. Oxygen reduction reaction activities

ORR activities of Co(OH)₂/rGO and Co₃O₄/rGO were carried out with rotating disk electrode (RDE) in a 0.1 M KOH electrolyte at a 5 mVs⁻¹ scan rate. Nitrogen (N₂) saturated electrolyte was used for comparison and the electrochemical activities were calculated by subtracted the performance in saturated electrolyte from O₂ to N₂. ORR activities were measured by a rotating disk electrode using rotating values 400, 625, 900, 1225, 1600 and 2025 rpm. ORR activities of Co(OH)₂/rGO and Co₃O₄/rGO were shown in Fig 20. The diffusion current layer of Co(OH)₂/rGO was stable, and the onset potential of this catalyst it was 0.86 V vs.RHE. The electron transfer number (n) was calculated by Koutecky-Levich equation^{61,62}:

$$B = 0.62 nFC_bD_o^{2/3}\nu^{-1/6}$$

Where, n is the number of electrons transferred in the ORR, F is the Faraday constant (96,485 Cmol⁻¹), C_b is the bulk concentration of O₂ (1.2 x 10⁻⁶ molcm⁻³), D_o is the diffusion coefficient of O₂ (1.9 x 10⁻⁵ cm²s⁻¹), and ν is the viscosity of the electrolyte. In the case of 0.1 M KOH, ν has been reported as 0.01 cm² s⁻¹. ω indicates the angular rotation rate of the electrode. Kinetic current density (j_k) was obtained from various voltages from the ORR curve (0.3 V to 0.45 V vs.RHE), and it was plotted as a function of $\omega^{-1/2}$. K-L plots showed linearity in Fig 20, and it could be concluded that the ORR for the two catalysts followed a four-electron transfer reaction.

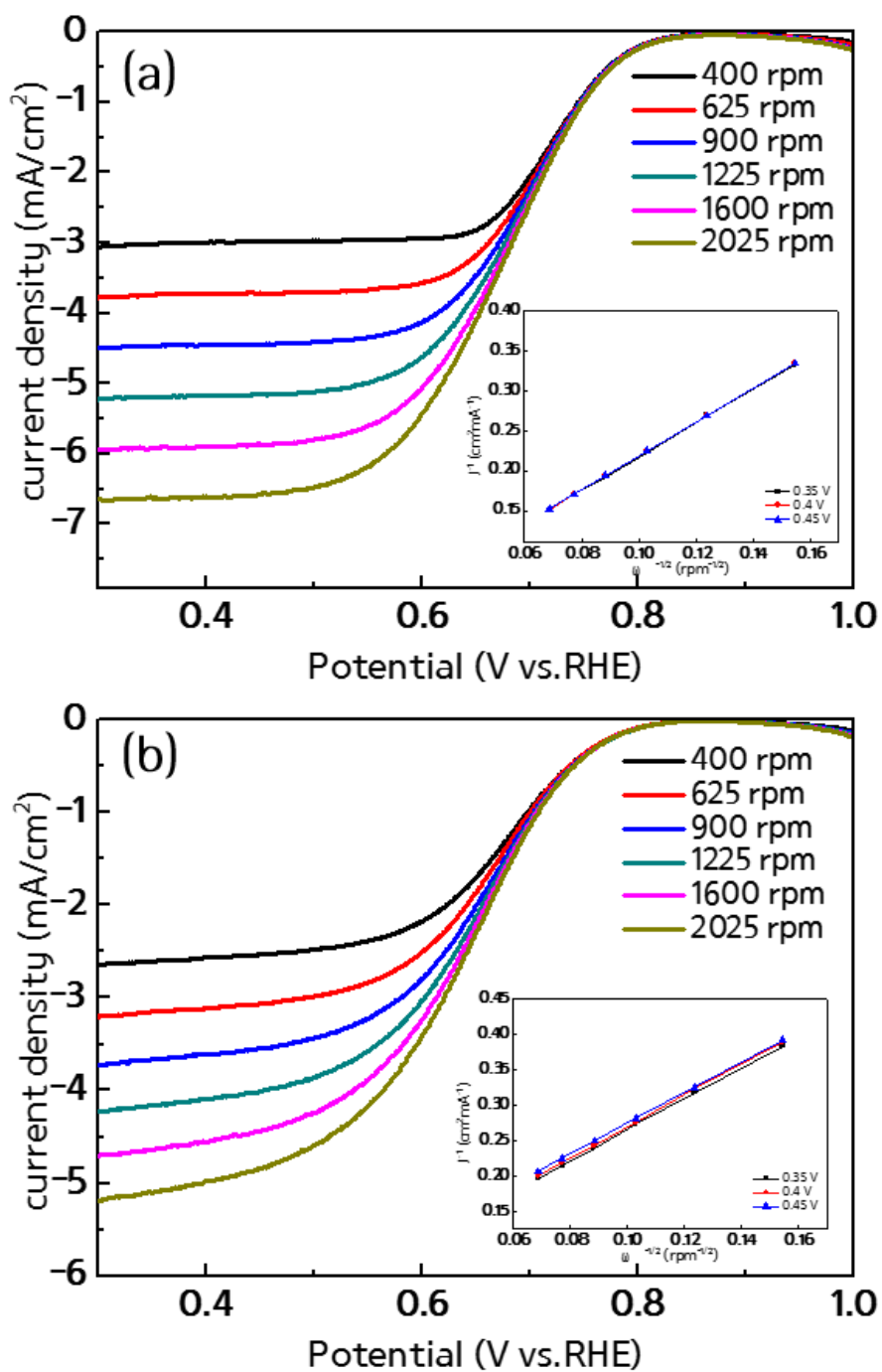
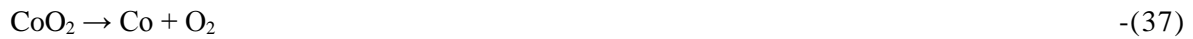


Fig. 20. RDE traces and Koutechy-Levich plot of (a) $\text{Co(OH)}_2/\text{rGO}$ and (b) $\text{Co}_3\text{O}_4/\text{rGO}$

3.8.2. Oxygen evolution reaction activities

To use the bi-functional catalyst, it should show not only good ORR activity but also good OER activity. To compare the OER activities of the two catalysts, a 1600 rpm rotating rate was selected. Before comparing the OER activities of the two catalysts, the OER activity of $\text{Co(OH)}_2/\text{rGO}$ was carried out the tendency enough to explain the OER mechanism in Fig 22a. There was oxidation reaction at 1.45 V vs.RHE, and the current increased after that potential in the first cycle. In the second cycle, the oxidation reaction disappeared at 1.45 V vs.RHE and similar amounts of current were generated after some potential as 1.7 V vs.RHE. The OER activity of $\text{Co}_3\text{O}_4/\text{rGO}$ was measured and had a similar shape with the second cycle of $\text{Co(OH)}_2/\text{rGO}$. This observation explained that Co(OH)_2 could be oxidized to cobalt oxide as the cycle increased in alkaline electrolyte with OER and it was shown in Fig. 21.



Co(OH)_2 oxidized to be Co^{3+} , which could be explained that Co_3O_4 had different oxidation state as Co^{2+} and Co^{3+} by spinel structure⁷³. It could demonstrate Co^{3+} is active state to make OER.

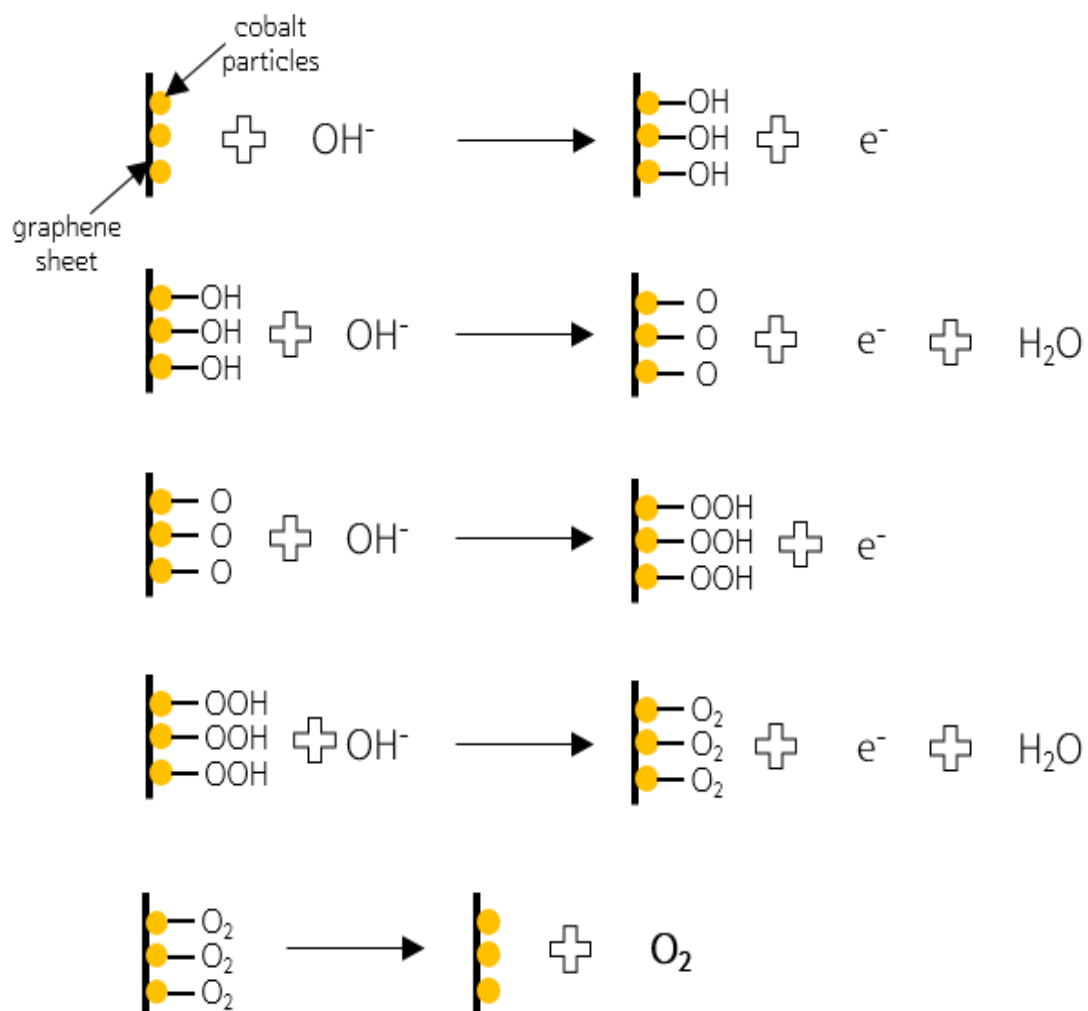


Fig. 21. The mechanism of OER on the surface of cobalt particles in alkaline solution.

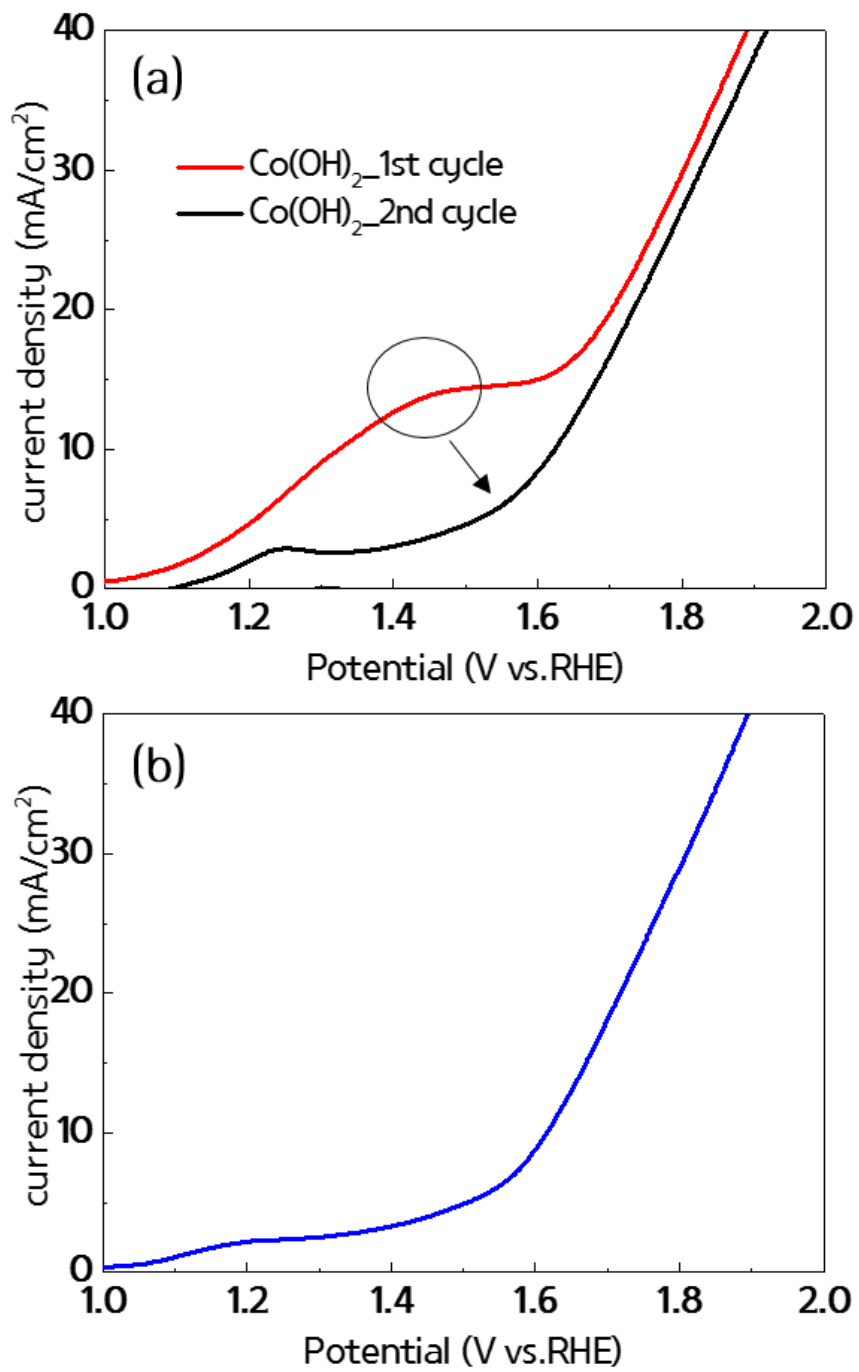


Fig. 22. OER activities of (a) Co(OH)₂/rGO and (b) Co₃O₄/rGO

To commercialize the OER catalyst, the current density of catalysts has to be analyzed. OER was mainly used for solar cells, and when the efficiency as 10 % of solar cell could be commercialized. To compare the solar cell, 10% efficiency of solar cells corresponded with 10 mAcm^{-2} of current density of electrochemical cell. When the current density of 10 mAcm^{-2} occurred, the potential of $\text{Co(OH)}_2/\text{rGO}$ and $\text{Co}_3\text{O}_4/\text{rGO}$ was 1.32 V vs.RHE and 1.61 V vs.RHE. During the OER experiment, bubbles on the surface of the electrode were observed. This made it difficult to continue doing more cycles.

The reason why half-wave potential was used for ORR standard potential was that it is already analyzed the oxidation-reduction reaction in electrochemical fields. The half-wave potential of $\text{Co(OH)}_2/\text{rGO}$ was slightly higher than that of $\text{Co}_3\text{O}_4/\text{rGO}$, that was 0.68 V vs.RHE was 40 mV higher than 0.64 V vs.RHE. The active OER potential of $\text{Co(OH)}_2/\text{rGO}$ and $\text{Co}_3\text{O}_4/\text{rGO}$ was 1.32 V vs.RHE and 1.61 V vs.RHE, respectively.

The oxygen electrode potential values of the two catalysts were 0.64 V vs.RHE of Co(OH)_2 and 0.97 V vs.RHE of $\text{Co}_3\text{O}_4/\text{rGO}$. These values were higher than commercial bi-functional catalysts such as iridium oxides (0.92 V), ruthenium oxides (1.01 V), and manganese oxides (1.04 V)^{3,4,30,63}. To maintain the cobalt hydroxide structure with increasing the potential and cycle was almost impossible. In other words, cobalt hydroxide was not a good material for bi-functional catalyst but a useful material to explain the OER mechanism.

IV. CONCLUSIONS

We had successfully synthesized hybrid catalysts as $\text{Co}_3\text{O}_4/\text{rGO}$, $\text{MnCo}_2\text{O}_4/\text{rGO}$ and $\text{Co}_3\text{O}_4/\text{NrGO}$ for bi-functional catalysts. There were differences in three catalysts: $\text{MnCo}_2\text{O}_4/\text{rGO}$ was doped manganese to cobalt oxide and $\text{Co}_3\text{O}_4/\text{NrGO}$ was doped nitrogen to reduced graphene oxide. Both catalysts affected only ORR activities. As we already discussed OER activity depends on oxidation state of catalytic materials. With doping, there is no change of oxidation state of catalytic material, just change in type of materials.

To improve OER activity, mechanism of OER was studied by $\text{Co}(\text{OH})_2/\text{rGO}$ and $\text{Co}_3\text{O}_4/\text{rGO}$. The hydrothermal process made a spinel structure for good activities, and $\text{Co}(\text{OH})_2/\text{rGO}$ that was not undergone hydrothermal process made an explanation for OER steps. Both of two catalysts were confirmed the difference by SEM, TEM, XRD and XPS. Electrochemical results of two catalysts demonstrated the possibility for commercialization as bi-functional catalyst. Based on our results, non-precious metal such as cobalt oxide could be good candidates as a catalyst for metal-air batteries and other renewable energy sources.

REFERENCES

- [1] Lee J.S., Kim S.T., Cao R. Choi N.S., Liu M., Lee K.T. and Cho J.P. "Metal-Air Batteries with High Energy Density: Li-Air versus Zn-Air." *Adv. Energy Mater*, 1, 2011, pp. 34-50
- [2] Simon P. and Gogotsi Y. "Materials for electrochemical capacitor" *Nat Mater*, 7(11), 2008, pp. 845-854
- [3] Chen G.Y., Bare S.R. and Mallouk T.E. "Development of Supported bi-functional electrocatalysts for unitized regenerative fuel cells" *J. Electrochem. Soc*, 149(8), 2002, pp.1092-1099
- [4] Zhang Y.J, Wang C. Wan N.F and Mao Z.Q, "Deposited RuO₂-IrO₂/Pt electrocatalyst for the regenerative fuel cell" *Int. J. Hydrogen Energy*, 32, 2007, pp. 400-404
- [5] Wang H., Robinson J.T., Diankov G. and Dai H. "Nanocrystal growth on graphene with various degrees of oxidation" *J. Am. Chem. Soc*, 132, 2010, pp. 3270-3271
- [6] Wang H.L., Casalongue H.S., Liang Y.Y. and Dai H.J "Ni(OH)₂ nanoplates grown on graphene as advanced electrochemical pseudocapacitor materials" *J. Am. Chem. Soc*, 132, 2010, pp. 7472-7477
- [7] Liang Y.Y., Wang H.L., Casalongue H.S. Chen Z. and Dai H.J "TiO₂ nanocrystals grown on graphene as advanced photocatalytic hybrid materials" *Nano Res*, 3, 2010, pp. 701-705
- [8] Li Y. "MoS₂ nanoparticles grown on graphene: An advanced catalyst for the hydrogen evolution reaction" *J. Am. Chem. Soc*, 133, 2011, pp. 7296-7299
- [9] Dong Y., He K., Yin L. and Zhang A. "A facile route to controlled synthesis of Co₃O₄ nanoparticles and their environmental catalytic properties" *Nanotechnology*, 18, 2007, pp. 435602-435607
- [10] Abraham K.M. and Jiang Z. "A Polymer electrolyte-based rechargeable Lithium/Oxygen battery" *Electrochem. Soc*, 143, 1996, pp. 1-5

- [11] Ogasawara T., Debart. A., Holzapfel, Novak P. and Bruce P. G. "Rechargeable Li₂O₂ electrode for lithium batteries" *J. Am. Chem. Soc.*, 128, 2006, pp. 1390-1393
- [12] Wang Z.L. Xu D. Xu J.J and Zhang X.B "Oxygen electrocatalysts in metal-air batteries: from aqueous to nonaqueous electrocatalysts", *Chem. Soc. Rev.*, 2013.
- [13] Gao X.P and Yang H.X. "Multi-electron reaction materials for high energy density batteries" *Energy environ. Sci.*, 3, 2010, pp. 174-189
- [14] Christensen P.A., Hamnett A. and Linares D. "Oxygen reduction and fuel oxidation in alkaline solution" *Phys. Chem. Chem. Phys.*, 13, 2011, pp. 5206-5214
- [15] Spendelow J.S and Wieckowshi A. "Electrocatalysis of oxygen reduction and small alcohol oxidation in alkaline media" *J. Phys. Chem. Chem. Phys.*, 9, 2007, pp. 2654-2675
- [16] Jorisen L. "Bifunctional oxygen/air electrodes" *Power Sources*, 155, 2006, pp. 23-32
- [17] Zhang P., Chen X.F., Lian J.S. and Jiang Q. "Functionalized hydrogen-bonding self-assembled monolayers grafted onto SiO₂ substrates" *J. Phys. Chem. C*, 116, 2012, pp. 17672-17680
- [18] Gao W., Chen X.F., Li J.C. and Jiang Q. "Is Au₅₅ or Au₃₈ cluster threshold catalyst for styrene epoxidation?" *J. Phys. Chem. C*, 114, 2010, pp. 1148-1153
- [19] Rasiyah P. and Tseung A.C.C. "The Role of the lower metal oxide/higher metal oxide couple in oxygen evolution reactions" *J. Electrochem. Soc.*, 131, 1984, pp. 803-808
- [20] Laoire Co.O., Mukerjee S., Abraham K.M., Plichta J. and Hendrickson M.A. "Fundamental Aspects of Oxygen Reduction in Non-aqueous Electrolytes: Formulation of a General Mechanism" *J. Phys. Chem. C*, 113, 2009, pp. 20127-20133
- [21] Laoire Co.O., Mukerjee S., Abraham K.M., Plichta J. and Hendrickson M.A. "Influence of Nonaqueous Solvents on the electrochemistry of Oxygen in the rechargeable Lithium-air battery" *J. Phys. Chem. C*, 114, 2010, pp. 9178-9186
- [22] Lu Y.C. and Shao-Horn Y. "Probing the reaction kinetics of the charge reactions of nonaqueous Li-O₂ batteries" *J. Phys. Chem. Lett.*, 4, 2013, pp. 93-99
- [23] McCloskey B.D., Bethune D.s., Shelby R.M., Girishkumar G. and Luntz A.C. "Solvents critical role in nonaqueous lithium-oxygen battery" *J. Phys. Chem. Lett.*, 2, 2011, pp.1161-1166

- [24] McCloskey B.D., Bethune D.s., Shelby R.M., Girishkumar G. and Luntz A.C. "On the efficacy of electrocatalysis in nonaqueous Li-O₂ batteries" *J. Am. Chem. Soc.*, 133, 2011, pp. 18038-18041
- [25] Kraytsberg A. and Ein-Eli Y. "Review on Li-air batteries-Opportunities, limitations and perspective" *J. Power Sources*, 196(3), 2011, pp. 886-893
- [26] Zhang T., Imanishi N., Shimonishi Y. Hirano A., Takeda Y., Yamamoto O. and Sammes N. "A novel high energy density rechargeable lithium/air battery" *Chem. Commun*, 46(10), 2010, pp. 1661-1663
- [27] Cao R., Lee J.S., Liu M. and Cho J. "Recent Progress in Non-Precious Catalyst for Metal-Air Batteries" *Adv. Energy Mater*, 2, 2012, pp. 816-829
- [28] Wang H., Cui L.F., Yang Y., Casalongue H.S., Robinson J.T, Liang Y., Cui Y. and Dai H. "Mn₃O₄-graphene Hybrid as a High-Capacity Anode Material for Lithium Ion Batteries" *J. Am. Chem. Soc.*, 132, 2010, pp. 13978-13980
- [29] Yang X.H and Xia Y.Y. "Partially fluorinated solvent as a co-solvent for the non-aqueous electrolyte of Li/air battery" *J. Power sources*, 196, 2011, pp. 2867-2870
- [30] Cnanamuthu D.S and Petrocelli J.V. "Electrocatalytic properties of mixed transition metal tellurides for oxygen reduction" *J. electrochem. Soc.*, 114, 1967, pp. 1036-1040
- [31] Trasatti S. "Electrocatalysis in anodic evolution of oxygen and chlorine" *Electrochim. Acta*, 29, 1984, pp. 1503-1512
- [32] Zoltowski P. Drazic K.M and Borkapic L. "Carbon-air electrode with regenerative short time overload capacity" *J. Appl. Electrochem*, 3, 1973, pp. 271-279
- [33] Mao L.Q., Zhang D., Sotomura T., Nakatsu K., Koshiha N. and Ohsaka T, "Mechanistic study of the reduction of oxygen in air electrode with manganese oxide as electrocatalysts" *Electrochim. Acta*, 48, 2003, pp. 1015-1021
- [34] Chen F., Shen J., Ji W., Tao Z. and Chen J. "Selective Synthesis of manganese oxide nanostructure for electrocatalytic oxygen reduction" *ACS Appl. Mater. Interfaces*, 1, 2009, pp. 460-466

- [35] Chen F., Su Y., Liang J., Tao Z. and Chen J. "MnO₂-based nanostructures as catalysts for electrochemical oxygen reduction in alkaline media" *Chem. Mater.* 22, 2010, pp. 898-905
- [36] Mirzaeian M. and Hall P.J. "Preparation of controlled porosity carbon aerogels for energy storage in rechargeable lithium oxygen batteries" *Electrochim. Acta*, 54, 2009, pp. 7444-7451
- [37] Mirzaeian M. and Hall P.J. "Characterizing capacity loss of lithium oxygen batteries by impedance spectroscopy" *J. Power Sources*, 195, 2010, p. 6817-6824
- [38] Yang X. H., He P., and Xia Y.Y. "Preparation of mesocellular carbon foam and its application for lithium/oxygen battery" *Electrochem. Commun.* 11, 2009, pp. 1127-1130
- [39] Lee J.S., Par G.S., Lee H.I., Kim S.T., Cao R.G., Liu M.L. and Cho J. "Ketjenblack carbon supported amorphous manganese oxide nanowires as highly efficient electrocatalyst for oxygen reduction reaction in alkaline solutions" *Nano Lett.*, 11, 2011, pp. 5362-5366
- [40] Beck F. "The redox mechanism of the chelate-catalysed oxygen cathode" *J. Appl. Electrochem.* 7, 1977, pp. 239-245
- [41] Shi C.N. and Anson F.C. "Catalytic pathways for the electroreduction of O₂ by Iron tetrakis porphyrin of Iron tetrapheylporphyrin adsorbed on edge plane pyrolytic graphite electrodes" *Inorg. Chem.* 29, 1990, pp. 4298-4305
- [42] Steiger B. and Anson F.C. "[5, 10, 15, 20-Tetrakisphenylporphyrinato]cobalt(II) immobilized on graphite electrode catalyzes the electroreduction of O₂ to H₂O, but the corresponding 4-cyano-2, 6-dimethylphenyl derivative catalyzes the reduction only to H₂O₂" *Inorg. Chem.* 36, 1997, pp. 4138-4140
- [43] Song E., Shi C.N. and Anson F.C. "Cobalt(II) hematoporphyrin IX and protoporphyrin IX complexes immobilized on highly dispersed titanium(IV) oxide on an cellulose microfiber surface" *Langmuir*, 14, 1998, pp. 4315-4320
- [44] Spendelow J.S. and Wieckowski A. "Electrocatalysis of oxygen reduction and small alcohol oxidation in alkaline media" *Phys. Chem. Chem. Phys.* 9, 2007, pp. 2654-2675

- [45] Zinola C.F., Arvia A.J., Estiu G.L and Castro E.A. "A Quantum chemical approach to the influences of platinum surface structure on the oxygen electroreduction reaction" *J. Phys. Chem*, 98, 1994, pp. 7566-7576
- [46] Ferreira K. N., Iversion T. M., Maghlaoui K., Barber J. and Iwata S, "Architecture of the photosynthetic oxygen-evolving center" *Science*, 303, 2004, pp. 1831-1838
- [47] Morita M., Iwakura C., Tamura H. "The anodic characteristics of massive manganese oxide electrode" *Electrochim Acta*, 24, 1979, pp. 357-362
- [48] Najafpour M.M., Ehrenberg T., Wiechen M. and Kurz P. "Calcium manganese oxides as biomimetic oxygen evolving catalysts" *Angew. Chem*, 49, 2010, pp. 2233-2237
- [49] Jiao F. and Frei H. "Nanostructured manganese oxide clusters supported on mesoporous silica as efficient oxygen evolving catalysts" *Chem. Commun*, 46, 2010, pp. 2920-2922
- [50] Gasteiger H.A., Kocha S.S., Sompalli B. and Wagner F.T. "Activity benchmarks and requirements for Pt, Pt-alloy, and non-Pt oxygen reduction catalysts for PEMFCs" *Appl. Catal*, 56, 2005, pp. 9-35
- [51] Limburg J., Vrettos J.S., Chen H.Y., Paula J.C., Crabtree R.H. and Brudvig G.W. "Speciation of the catalytic oxygen evolution system" *J. Am. Chem. Soc*, 123, 2001, pp. 423-432
- [52] Huang X., Zeng Z.Y., Fan Z.X., Liu J.Q. and Zhang H. "Graphene-based electrodes" *Adv. Mater*, 24, 2012, pp. 5979-6004
- [53] Huang X., Gi X.Y., Boey F. and Zhang H., "Graphene-based composites" *Chem. Soc. Rev*, 41, 2012, pp. 666-686
- [54] Nardecchia S., Carriazo D., Ferrer M.L., Cuitierrez C. and Monte F.D, "Three dimensional macroporous architectures and aerogels built of carbon nanotubes and/or graphene" *Chem. Soc. Rev*, 42, 2013, pp. 794-830
- [55] Hummers W.S., Offeman R.E. "Graphene nanoelectronics: Metrology, Synthesis, Properties and applications" *J. Am. Chem. Soc*, 80, 1957, pp. 1339-1342

- [56] Lee J.W., Hall A.S., Kim J.D. and Mallouk T.E "A Facile and Template-Free Hydrothermal Synthesis of Mn₃O₄ Nanorods on Graphene Sheets for Supercapacitor Electrodes with Long Cycle Stability" *Chem. Mater*, 24, 2012, pp. 1158-1164
- [57] Liang Y., Li Y., Wang H., Zhou J., Wang J., Regier T. and Dai H. "Co₃O₄ nanocrystals on graphene as a synergistic catalyst for oxygen reduction reaction" *Nature mater*, 10, 2011, pp. 780-786
- [58] Mayrhofer K.J. "Measurement of oxygen reduction activities via the rotating disc electrode method: From Pt model surfaces to carbon-supported high surface area catalysts" *Electrochim. Acta*, 53, 2008, pp. 3181-3188
- [59] Subramanian N.P., Si X.G., Nallathambi B., Kumaraguru S.P., Colon-Mercado H., Wu G. Lee J.W. and Popov B.N. "Nitrogen-Modified Carbon-Based Catalysts for Oxygen Reduction Reaction in Polymer Electrolyte Membrane Fuel Cells" *J. Power Sources*, 188, 2009, pp. 38-44
- [60] Oh H.S., Oh J.G., Lee W.H., Kim H.J. and Kim H. "The influence of the structural properties of carbon on the oxygen reduction reaction of nitrogen modified carbon based catalysts" *Int. J. Hydrogen Energy*, 36, 2011, pp. 8181-8186
- [61] Liang Y., Wang H., Chang W., Hong G., Li Y., Gong M., Xie L., Zhou J., Wang J., Regier T.Z., Wei F., Dai H. "Surface structure dependent electrocatalytic activity of Co₃O₄ anchored on graphene sheets toward oxygen reduction reaction" *J. Am. Chem. Soc*, 134, 2012, pp. 15849-15857
- [62] Jianbo X., Ping G., Zhau T.S. "Non-precious Co₃O₄ nano-rod electrocatalyst for oxygen reduction reaction in anion-exchange membrane fuel cells" *Energy Environ. Sci*, 5, 2012, pp. 5333-5339
- [63] Matsumoto Y. and Sato E. "Electrocatalytic properties of transition metal oxides for oxygen evolution reaction" *Mater. Chem. Phys*, 14, 1986, pp. 397-426
- [64] Fangyi C., Jian S., Bo P., Yuede P., Zhanliang T. and Jun C. "Rapid-room temperature synthesis of nanocrystalline spinels as oxygen reduction and evolution electrocatalysts" *Nature Chemistry*, 3, 2011, pp. 79-84

- [65] Jakub A., Caleb M., Ying-Chau L. and Jay A. "Interpretation of optoelectronic transient and charge extraction measurements in de-sensitized solar cells" *Chem. Mater.* 25, 2013, pp. 1922-1926
- [66] Dong U.L., Bae J.K. and Zhongwei C. "One-pot synthesis of a mesoporous NiCo₂O₄ nanoplatelet and graphene hybrid and its oxygen reduction and evolution activities as an efficient bi-functional electrocatalysts" *J. Mater. Chem. A*, 1, 2013, pp. 4754-4762
- [67] Taylor R.J. and Humffray A.A. "Electrochemical studies on glassy carbon electrodes: Oxygen reduction in solutions of high pH (pH > 10)" *J. Electrochem. Soc.*, 106, 1959, pp. 56-62
- [68] Zhang M., Yan Y., Gong K., Mao L., Guo Z. and Chen Y. "Electrostatic layer by layer assembled carbon nanotube multilayer film and its catalytic activity for oxygen reduction reaction" *Langmuir*, 20, 2004, pp. 8781-8785
- [69] Appel M. and Appleby A.J. "A ring disk electrode study of the reduction of oxygen on active carbon in alkaline solution" *Electrochim. Acta*, 23, 1978, pp. 1243-1246
- [70] Hogan. C. and Michael "Density of States of an Insulating Ferromagnetic Alloy" *Physical Review*, 188(2), 1969, pp. 870-874
- [71] Baliga B. J. *Modern Power Devices*, John Wiley & Sons, New York, 1987, 32 pages
- [72] Sproul A.B and Green M.A "Intrinsic concentration, effective densities of states and effective mass in silicon" *Journal of Applied Physics*, 67(6), 1990, pp. 2941-2944
- [73] Jakub A. K., Caleb M. H., Ying C.L., and Jay A. S. "Deposition of β -Co(OH)₂ Films by Electrochemical Reduction of Tris(ethylenediamine)cobalt(III) in Alkaline Solution. " *Chem. Mater.* 25, 2013, pp. 1922-1926 [1] Lee J.S., Kim S.T., Cao R. Choi N.S., Liu M., Lee K.T. and Cho J.P. "Metal-Air Batteries with High Energy Density: Li-Air versus Zn-Air. " *Adv. Energy Mater.*, 1, 2011, pp. 34-50

요 약 문

비금속 물질을 이용하여 효율적인 산소 환원 반응과 산소 생성 반응을 위한 촉매 연구

본 논문은 화석 연료의 고갈과 환경 오염의 문제로 대두되고 있는 신재생에너지원의 한 종류인 ‘금속-공기 전지’의 촉매 연구에 대해 다룬다. 대기 중의 공기를 이용하여 전기 에너지를 생산할 수 있다는 큰 이점을 지니고 있는 ‘금속-공기 전지’ 중에서도 양극에 사용되는 촉매에 관한 연구가 필요하다. 금속의 산화 반응이 일어나는 음극에 비하여, 양극은 공기의 산화/환원 반응으로 내구성과 효율에 관한 문제점이 제기된다. 백금, 이리듐, 루테튬 산화물이 촉매로 이용되고 있으나, 비싼 가격과 구하기 어렵다는 단점으로 대체 물질이 요구된다. 본 연구에서는 코발트 산화물을 이용하여 산소 산화/환원 반응의 효율을 평가하였다. 효율을 증가시키기 위하여 코발트 산화물의 성질을 변화시킬 수 있는 망간과 질소 도핑을 이용하여 효율의 차이를 비교하였다. 산소 환원 반응에 비해 상대적으로 연구가 부족한 산소 산화 반응의 개념을 설명하기 위하여 다른 형태의 코발트 산화물을 이용하여 실험을 진행 하였다. 촉매 물질의 특성을 평가하는 방법으로 물리적, 화학적, 전기화학적 방법이 이용되었으며, 이를 바탕으로 ‘금속-공기 전지’의 상업화의 가능성을 제시할 수 있는 효율적인 촉매 연구가 지속적으로 진행되어야 할 것이다.

핵심어 :

산소 산화/환원 촉매, 산소 환원 반응, 산소 산화 반응, 코발트 산화물